▌**Reaction Mechanism** |*Hot Paper*|

Enantioselective Halogenative Semi-Pinacol Rearrangement: Extension of Substrate Scope and Mechanistic Investigations

Fedor Romanov-Michailidis,[b] Maria Romanova-Michaelides,[c] Marion Pupier,[b] and Alexandre Alexakis*[a]

Abstract: The present Full Paper article discloses a survey of our recent results obtained in the context of the enantioselective halogenation-initiated semi-pinacol rearrangement. Commencing with the fluorination/semi-pinacol reaction first and moving to the heavier halogens (bromine and iodine) second, the scope and limitations of the halogenative phase-transfer methodology will be discussed and compared. An extension of the fluorination/semi-pinacol reaction to the ring-expansion of five-membered allylic cyclopenta-nols will be also described, as well as some preliminary results on substrates prone to desymmetrization will be given. Finally, the present manuscript will culminate with a detailed mechanistic investigation of the canonical fluorination/semi-pinacol reaction. Our mechanistic discussion will be based on in situ reaction progress monitoring, complemented with substituent effect, kinetic isotopic effect and non-linear behaviour studies.

Introduction

In the course of the last ten years, it has been extensively demonstrated that ionic catalysts incorporating at least one chiral ion are able to render enantioselective transformations proceeding through reaction intermediates bearing an opposite electrostatical charge.[1] More specifically, in the context of asymmetric anionic counterion-directed catalysis, the conjugate bases of enantiopure 1,1′-bi-2-naphthol (BINOL)-derived phosphoric acids have been recently disclosed as privileged chiral anions.[2] The combination of these elements has now blossomed into the rich field of ion-pairing catalysis.

Anslyn and Dougherty have provided the following definition of an ion pair:[3] "An ion pair is defined to exist when a cation and anion are close enough in space that the energy associated with their electrostatic attraction is larger than the thermal energy ($k_B T$) available to separate them." Despite this definition, the frontier between strict ion-pairing and other weak intermolecular interactions is rather shallow, and the term "ion pair" can be used to describe an ensemble of non-covalent binding forces that keep two oppositely charged species associated in solution (Figure 1). The terms contact, tight, or intimate ion pair and solvent-separated or loose ion pair have become well known in the chemical community.[4]
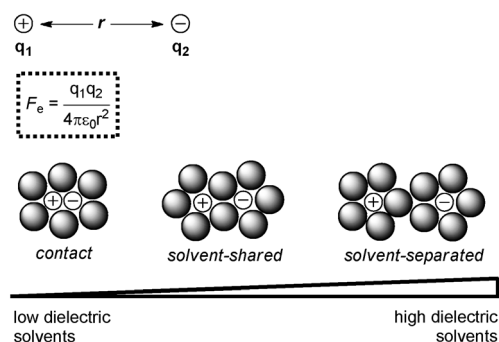

Figure 1. Coulomb's law and the types of ion-pairing in solution.

Historically, the ability of chiral non-racemic species to influence the enantioselectivity of a chemical transformation through ion-pairing interactions has been initially demonstrated by the field of asymmetric phase-transfer catalysis.[5] The first use of such systems can be traced back to 1984, when Merck scientists achieved a highly enantioselective alkylation of indanone enolates, ion-paired with chiral quaternary ammonium cations.[6]

It is curious to note that the reversed polarity stratagem, notably ion-pairing of an achiral/prostereogenic cationic reagent/intermediate with an enantiopure chiral anionic catalyst lagged rather far behind and was only recently applied to asymmetric catalysis.[7,8,9] Of particular interest to us are these

[a] Prof. Dr. A. Alexakis
Department of Organic Chemistry
University of Geneva
Quai Ernest Ansermet 30, 1211 Geneva 4 (Switzerland)
E-mail: Alexandre.Alexakis@unige.ch

[b] Dr. F. Romanov-Michailidis, M. Pupier
Department of Organic Chemistry
University of Geneva
Quai Ernest Ansermet 30, 1211 Geneva 4 (Switzerland)

[c] M. Romanova-Michaelides
Department of Biochemistry
University of Geneva
Quai Ernest Ansermet 30, 1211 Geneva 4 (Switzerland)

These are not the final page numbers! ↗↗

last three examples, in which the authors took a new approach in the form of establishing a phase separation between the organic solution phase (containing the substrate together with the chiral lipophilic anion) and the solid phase (containing the insoluble stoichiometric cationic reagent). The poor solubility of the latter precluded background reaction but did allow the reaction with its salt with the chiral lipophilic anion.

The regio- and stereocontrolled functionalization of carbon–carbon double bonds **1** is of primordial importance in organic synthesis. Transition-metal-free electrophilic activation of olefins has been largely dominated by halofunctionalization reactions.[10] These reactions involve the capture of transient haliranium ions **2**, formed from olefin/dihalogen association, by inter- or intramolecular nucleophiles (Figure 2).[11]
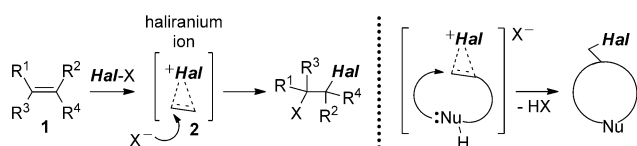

Figure 2. Electrophilic halofunctionalization of alkenes, and the special case of an halocyclization reaction.

The halocyclization process (intramolecular nucleophile trapping) represents the most studied halofunctionalization reaction.[12] In sharp contrast to the exhaustively studied bromocyclization process,[13, 14a,b] engineering enantioselectivity in fluoro-,[8, 9, 15] chloro-,[16] and iodocyclization[14] reactions remains challenging and lacks generality in terms of substrate scope. This constitutes an important handicap to the synthetic community due to the primordial role of fluorinated[17] and iodinated[18] organic molecules in natural products, pharmaceuticals and agrochemicals. Iodinated compounds are also valuable precursors that provide access to more complex molecular frameworks.[19]

Even less studied is the related halogenation-initiated semipinacol rearrangement. In this last reaction, the transiently formed α-hydroxy haliranium ion **4** undergoes a Wagner–Meerwein alkyl migration, leading to the formation of synthetically prized β-halogenated ketones.[20]

Whereas the chlorination- and bromination-initiated Wagner–Meerwein rearrangements of electron-rich cyclic enol ethers were recently shown to be amenable to asymmetric catalysis,[21] the development of truly enantioselective catalytic fluorination-[22] and iodination-initiated variants remains a great challenge.

Reasoning that the postulated haliranium ion intermediate **4** bears a net positive charge (Figure 3), we were interested to see whether a chiral anion (derived from a BINOL-phosphoric acid, for example) could induce asymmetry into the subsequent Wagner–Meerwein rearrangement step.

The transposition of simple allylic alcohols **3** was of particular interest to us, as it would lead to the formation of valuable all-carbon quaternary stereogenic centres. The present Full Paper will deal with the description of the scope and limitations of the halogenation-initiated Wagner–Meerwein rear-
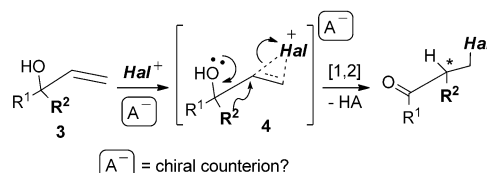

Figure 3. Concept behind halonium-ion-promoted Wagner–Meerwein transposition of allylic alcohols, and the idea of inducing chirality by means of a chiral counterion. Hal = F, Cl, Br or I.

rangements, operating through anionic phase-transfer technology. The key practical aspects of the title transformation, such as reaction optimization studies and the establishment of a substrate scope will be combined with mechanistic aspects, such as kinetic and isotopic kinetic data. Combined with linear free energy relationships, this study will culminate at a reasonable picture of the reaction mechanism.
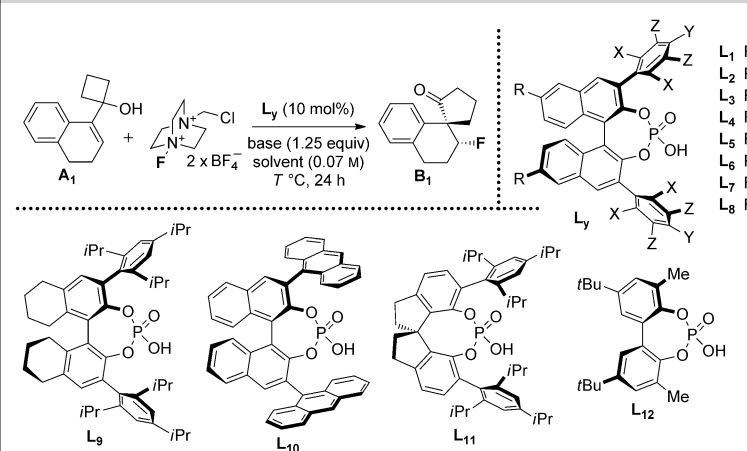
Results and Discussion

With a small library of enantiopure (R_a)-BINOL-derived, 3,3′-bis-aryl disubstituted phosphoric acids L_y ($y = 1$–12) in hand, reaction optimization studies were carried out next.[23] Optimization experiments were carried out with the strained allylic alcohol A_1, Selectfluor as the fluorinating reagent, and the set of acids L_y (see Table 1).

In the course of the preliminary catalyst screening performed in toluene at ambient temperature, the employment of highly sterically congested phosphoric acids $L_{4–6}$, related to the notorious (R_a)-TRIP (TRIP = 3,3′-bis(2,4,6-triisopropylphenyl)-1,1′-binaphthyl-2,2′-diyl hydrogenphosphate) scaffold,[24] turned out to be crucial for accessing practical enantioselectivities (ca. 70 % ee) of the product β-fluoro spiroketone B_1 (Table 1, entries 4–6). Interestingly, phosphoric acids bearing isopropyl (L_4) and cyclopentyl (L_6) substituents at positions X and Y outperformed acid L_5 that bears cyclohexyl groups at these same positions. The addition of Na_2CO_3 base turned out to be detrimental for the success of the title fluorination-induced semi-pinacol rearrangement, in terms of both the yield and the enantioselectivity. Thus, when employing phosphoric acid L_4 in the absence of the sodium carbonate additive (entry 8), a significant drop in conversion and enantiomeric excess was noted. This observation proves that it is the conjugate base of the acidic precatalyst, a chiral lipophilic phosphate anion, which is the catalytically active species in the title reaction.

The fact that our reaction obeys the chiral anion phase-transfer paradigm (PTC) was supported by the complete loss of reactivity in the non-polar toluene solvent observed in the absence of the phosphoric acid promoter (Table 1, entry 9). Nevertheless, the reactivity could be recovered when passing to the more polar acetonitrile solvent, a solvent that is known to solubilize Selectfluor to some extent (entry 10). In this case, the recovered β-fluoro spiroketone B_1 was of course racemic.

It is important to point out here that both the enantioselectivity as well as the diastereoselectivity of the present transformation are controlled by the catalyst structure. Thus, racemic

↖↖ These are not the final page numbers!

Table 1. Preliminary screening of the phosphoric acid catalysts.[a]

L$_1$	R = X = Y = Z = H
L$_2$	R = H, X = Y = Z = F
L$_3$	R = H, X = Z = H, Y = tBu
L$_4$	R = H, X = Y = iPr, Z = H
L$_5$	R = H, X = Y = c-C$_6$H$_{12}$, Z = H
L$_6$	R = H, X = Y = c-C$_5$H$_{10}$, Z = H
L$_7$	R = n-C$_8$H$_{17}$, X = Y = iPr, Z = H
L$_8$	R = TIPS, X = Y = iPr, Z = H

Entry	L$_x$	T [°C]	Base	Solvent	Yield [%][b]	d.r.[c]	e.r.[d]
1	L$_1$	25	Na$_2$CO$_3$	toluene	87	20:1	68:32
2	L$_2$	25	Na$_2$CO$_3$	toluene	35	10:1	57:43
3	L$_3$	25	Na$_2$CO$_3$	toluene	82	>20:1	63:37
4	L$_4$	25	Na$_2$CO$_3$	toluene	96	>20:1	86.5:13.5
5	L$_5$	25	Na$_2$CO$_3$	toluene	74	>20:1	82.5:17.5
6	L$_6$	25	Na$_2$CO$_3$	toluene	89	>20:1	86.5:13.5
7	L$_{12}$	25	Na$_2$CO$_3$	toluene	62	6:1	50:50
8	L$_4$	25	–	toluene	19[e]	>20:1	61:39
9	–	25	Na$_2$CO$_3$	toluene	trace	n.d.	n.d.
10	–	25	Na$_2$CO$_3$	acetonitrile	82	3:2	50:50

[a] Reaction conditions: a solution of allylic alcohol **A$_1$** (0.20 mmol, 1.0 equiv), chiral phosphoric acid **L$_x$** (0.02 mmol, 10 mol%), powdered Selectfluor (0.30 mmol, 1.5 equiv), and powdered Na$_2$CO$_3$ (0.25 mmol, 1.25 equiv) in anhydrous solvent (3.0 mL, 0.07 M) was stirred vigorously at 25 °C for 24 h. [b] Isolated yields after flash chromatography. [c] Determined by ^{1}H NMR spectroscopy of unpurified reaction mixtures. [d] Determined by chiral HPLC analysis of purified compounds. [e] ^{1}H NMR spectroscopy conversion. n.d. = not determined.

83% *ee*). Finally, even though the solvents tested were rigorously dried prior to use, an attempt to sequester residual water by the addition of 4 Å molecular sieves had a deleterious effect on the chemical yield of the reaction (67% yield).

Having checked single nonpolar solvents as appropriate reaction media, binary (1:1 (*v/v*) combination) solvent mixtures were examined next. In this regard, it turned out that employing a 1:1 mixture of fluorobenzene and *n*-hexane led to a noticeable increase in the level of asymmetric induction (up to 86% *ee*). Coupled with changing of the basic additive from Na$_2$CO$_3$ to Na$_3$PO$_4$, lowering of the reaction temperature to −20 °C and increasing of the reaction time to 48 h, these adjustments led to an increase of the enantioselectivity obtained with phosphoric acid **L$_4$** to 91% *ee*.

Furthermore, increasing the concentration of allylic alcohol **A$_1$** from 0.07 to 0.1 M led to

reactions (carried out with Selectfluor in acetonitrile without any phosphoric acid, Table 1, entry 10) gave quasi 1:1 mixtures of diastereisomers. Additionally, the diastereoselectivity was significantly reduced under PTC conditions as well, when employing the lipophilic but achiral phosphoric acid **L$_{12}$** (entry 7). Consequently, the catalyst structure not only controls the initial formation of the fluorinated stereogenic centre, but also participates in the second (alkyl migration) step.

In an attempt to increase the enantioselectivity of the fluorination-induced semi-pinacol rearrangement, the solvent of the reaction was varied while keeping the same chiral phosphoric acid catalyst (**L$_4$**) (see the Supporting Information).

Among the numerous single solvents tested, highly hydrophobic but yet strongly solubilizing (high polarizability) solvents such as toluene, fluorobenzene, and diisopropylether were better than hydrophobic solvents of lower solubilizing ability (cyclohexane). Since non-polar solvents favour strong ion-pairing interactions, the present reaction constitutes an example of chiral anion phase-transfer catalysis (PTC), in which a lipophilic chiral anion extracts the insoluble cationic fluorination reagent into the organic layer, thus rendering it chiral. The best solvent in terms of the enantioselectivity of the process turned out to be fluorobenzene. Importantly, decreasing the reaction temperature to 0 °C had a beneficial effect on the stereoselectivity of the fluorination/semi-pinacol sequence (up to

a higher chemical yield of the product β-fluoro spiroketone **B$_1$**, concomitantly with a slight drop of the enantiomeric excess (Table 1, entry 6). An optimal concentration of 0.07 M and a temperature of −20 °C were found as a compromise for catalyst **L$_4$**, affording **B$_1$** with perfect diastereo- and enantioselectivity.

The isolated yield of β-fluoro spiroketone **B$_1$** could be further increased when employing the more lipophilic phosphoric acid catalysts **L$_{6–9}$** (Table 1, entries 11–13). This is again in accord with the PTC mechanism, as the more lipophilic chiral anions derived from **L$_{6–9}$** are able to extract the cationic fluorination reagent more readily. In these last three cases, the catalyst loading could be decreased to 5 mol%, albeit at the expense of the reaction time. Since the use of catalyst **L$_6$** led to product **B$_1$** with the highest level of enantioinduction (92% *ee*) and perfect diastereoselectivity (>99:1 d.r.), this chiral phosphoric acid was selected as optimal for further studies.

With a set of optimal reaction conditions in hand, the substrate scope of the title transformation was studied next. To this end, strained allylic alcohols **A$_y$** (prepared according to experimental procedures described above) were stirred together with Selectfluor, Na$_3$PO$_4$ and chiral phosphoric acid **L$_6$** under our previously established reaction conditions (Scheme 1).

Both three- (*n* = 0, products **B$_{11–18}$**) and four-membered (*n* = 1, products **B$_{1–10}$**) allylic alcohols turned out to be amenable to

These are not the final page numbers! ↗↗
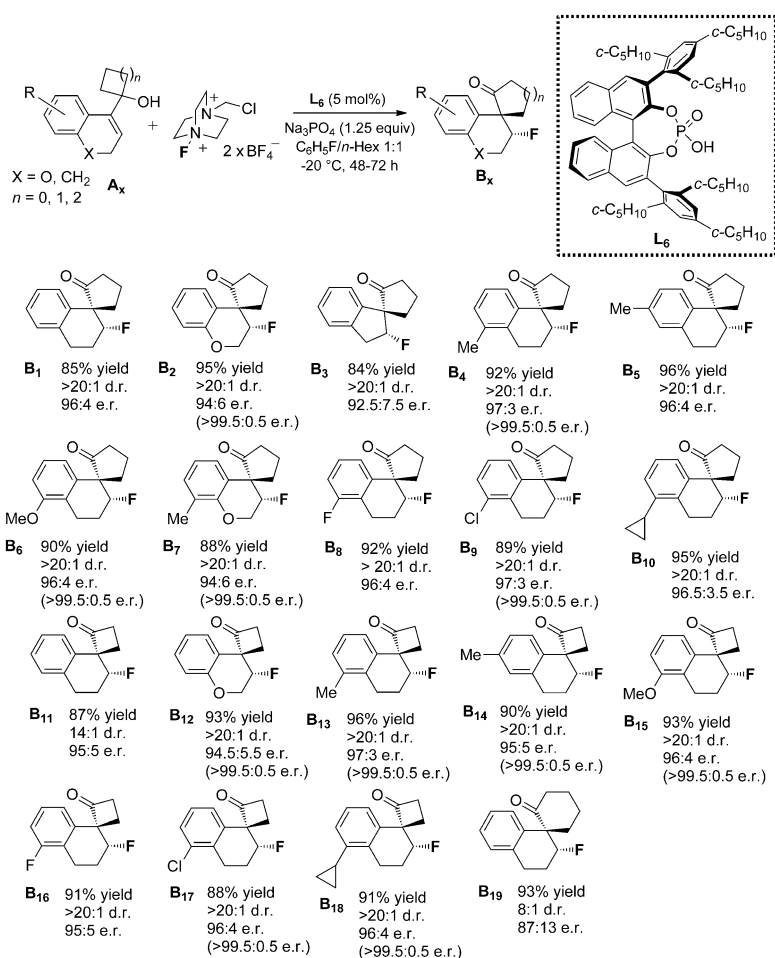
Scheme 1. Substrate scope of the fluorination-induced semi-pinacol rearrangement. The values in parentheses show enantiomer ratios after recrystallization.

enantioselective ring expansion, which occurred equally well with scaffolds based on dihydronaphthalene (X=CH$_2$, for example, **B$_1$**) as well as chromene (X=O, for example, **B$_2$**) ring systems. Concerning the substituent tolerance, electron-releasing (alkoxy-, products **B$_{6,15}$**), electron-neutral (alkyl-, products **B$_{4,5,10,13,14,18}$**), as well as moderately electron-withdrawing (halogen-, products **B$_{8,9,16,17}$**) groups were equally well tolerated when positioned at the C6-position of the dihydronaphthalene/chromene scaffold. A methyl substituent was also tolerated when placed at the C5-position of the dihydronaphthalene scaffold (products **B$_{5,14}$**).

The product β-fluoro spiroketones **B$_y$** were isolated in good to excellent yields, and in all cases the products displayed perfect d.r. (>20:1) and high e.r. (between 94:6 and 97:3) values. In many cases, the recovered β-fluoro spiroketones could be recrystallized from *n*-hexane/Et$_2$O, giving access to enantiomerically pure material. Fortunately, even product **B$_3$**, based on the indene (X=nothing) scaffold was obtained as a single diastereomer and with an encouraging 92.5:7.5 e.r. The sole disappointment came with β-fluoro spiroketone **B$_{19}$**, which resulted from ring-expansion of the five-membered (*n*=2) allylic al-

cohol **A$_{19}$**. For this last case, the diastereoselectivity of the reaction dropped to 8:1 d.r., while the enantioselectivity was reduced to 87:13 e.r. A slightly different catalytic system based around the (*R$_a$*)-SPINOL-derived phosphoric acid (**L$_{11}$**) (SPINOL= 1,1′-spirobiindane-7,7′-diol) was devised to deal with these challenging cases (vide infra).

One important limitation of the fluorination/semi-pinacol rearrangement methodology was discovered when subjecting allylic alcohols **A$_{19}$**, **A$_{20}$** and **A$_{21}$** to the optimized reaction conditions. All three of these substrates possess substituents (MeO, F and Cl, respectively) with lone pairs at the C5-position of the dihydronaphthalene ring. Consequently, these substituents are capable of direct resonance interaction with the developing benzylic carbocation at the transition structure issued from the fluorination step. This additional stabilization might in turn lead to an increase of the lifetime of the carbocationic intermediate, ultimately resulting in deterioration of the stereoselectivity of the process (Scheme 2). Indeed, for substrate **A$_{19}$** a decrease in the diastereomer ratio of the corresponding β-fluoro spiroketone **B$_{19}$** can be observed (9:2 d.r.), while the enantiomer ratio remains rather high for both diastereomers. On the other hand, for substrates **A$_{20}$** and **A$_{21}$**, a concomitant drop in enantioselectivity is also observed.

The second important limitation in terms of substrate scope is observed with dihydronaphthalene-based cyclobutanols that
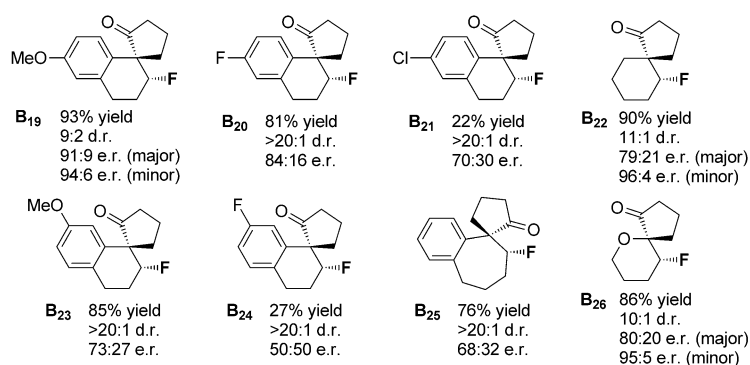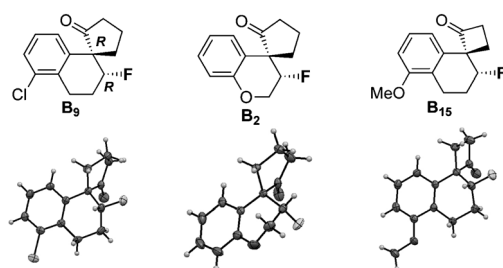

Scheme 2. Scope limitations of the fluorination-induced semi-pinacol rearrangement methodology.

bear substituents at the C4-position (substrates A_{23} and A_{24}, Scheme 2). In this case, a significant drop in the level of asymmetric induction occurs for both electron-releasing (MeO, substrate A_{23}, 73:27 e.r.) as well as electron-withdrawing (F, substrate A_{24}, 50:50 e.r.) substituents. The third and final limitation of our fluorination/semi-pinacol rearrangement cascade occurs when the dihydrobenzoazulene-based cyclobutanol A_{25} is employed as a substrate. While the corresponding β-fluoro spiroketone B_{25} was isolated in good chemical yield and as a single diastereomer, the enantiomer ratio was disappointingly low (68:32 e.r.).

Furthermore, at this stage, we were unable to extend our asymmetric methodology to allylic alcohols lacking the aromatic ring. For example, substrates based on dihydropyrane A_{26} or cyclohexene A_{22} scaffolds furnished the awaited β-fluoro spiroketones B_{26} and B_{22} in good yields but with only moderate stereoselectivities (Scheme 2). This is probably due to the inefficient docking of these substrates into the catalyst's chiral pocket (importance of π–π stacking interactions?).

Unambiguous assignment of relative and absolute configurations of the products was made possible after carrying out X-ray diffraction studies on single crystals grown from β-fluoro spiroketones B_9, B_2 and B_{15} (see Scheme 3).

Figure 4. Stereochemical rationale for the observed *Re*-face fluorination with a R_a-configured phosphate anion.

Scheme 3. Relative and absolute configurations of selected β-fluoro spiroketones, as determined by X-ray crystallography. Thermal ellipsoids are set at the 50% probability level.

Based on these X-ray crystal structures as well as on the model proposed by Simon and Goodman for BINOL-phosphoric acid-catalyzed reactions of imines,[25] we present here a rationale for the observed absolute and relative stereochemistries (Figure 4). According to our model, the positively charged Selectfluor reagent occupies the vacant lower-left quadrant of the catalyst, while establishing an ionic bridge with the negatively charged phosphoroyl oxygen atom. Presumably, the allylic cyclobutanol then establishes a hydrogen bond with the second phosphoroyl oxygen atom, while fitting the bulk of the dihydronaphthalene ring into the vacant upper-right quadrant. Consequently, the fluoronium bridge is formed at the *Re*-face
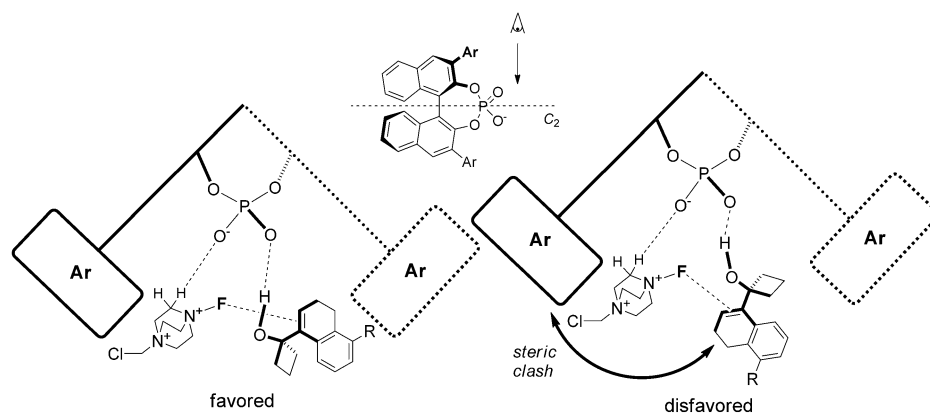
of the carbon–carbon double bond of the substrate, and migration occurs *anti* relative to the leaving group. From this model, we could speculate that the high tolerance towards substitution at positions C5 and C6 of the dihydronaphthalene ring observed experimentally is a consequence of these positions ending up in the vacant upper-right quadrant of the catalyst's chiral pocket. On the other hand, substituents at the C4-position would clash with the Ar groups and preclude optimal alignment of substrate and catalyst.

It is important to point out that the sense of absolute induction for our transformation is inversed when compared to the previously reported fluorocyclization of Toste and co-workers. If, in the case of the semi-pinacol rearrangement, *Re*-face fluorination takes places with a R_a-configured phosphate anion, an identically configured phosphate anion induces *Si*-face fluorination in the case of the fluorocyclization reaction.[8] Clearly, this deviation within the sense of chiral induction is due to an inversion in the preferred binding mode to the catalyst. While the model presented on the left (Figure 4) holds true for our case, it is the model on the right that is preferred when a different substrate is used. Such a switch in the binding preference is presumably caused by a conformational restriction that is present in our substrate and absent in Toste's one. The conformational restriction for tertiary allylic alcohols poised for a Wagner–Meerwein transposition comes from the positioning of the hydroxyl group synclinal to the alkene as to ensure the required orthogonality between the migrating C—C σ-bond and the π orbital of the alkene.

The herein disclosed enantioselective fluorination/semi-pinacol rearrangement cascade was readily amenable to scale-up. In one experiment, allylic alcohol A_{15} (540 mg, 2.5 mmol) was converted into the corresponding β-fluoro spiroketone B_{15} with excellent stereoselectivity and as low as 2.5 mol% loading of catalyst L_6 (Scheme 4). The desired product could be recovered in diastereo- and enantiomerically pure form with 78% isolated yield after a single recrystallization from *n*-hexane/Et$_2$O.

Furthermore, a selection of strained β-fluoro spirocyclobutanones ($B_{11–16}$) underwent smooth Baeyer–Villiger oxidation to the corresponding fluorinated spiro-γ-lactones $C_{11–16}$ in excellent chemical yield and with complete retention of relative and
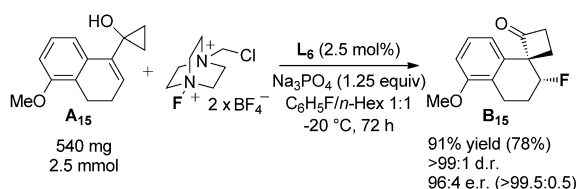
Scheme 4. Scale-up of the catalytic enantioselective fluorination-induced semi-pinacol rearrangement. The values in brackets show yields and enantiomeric ratios after recrystallization.
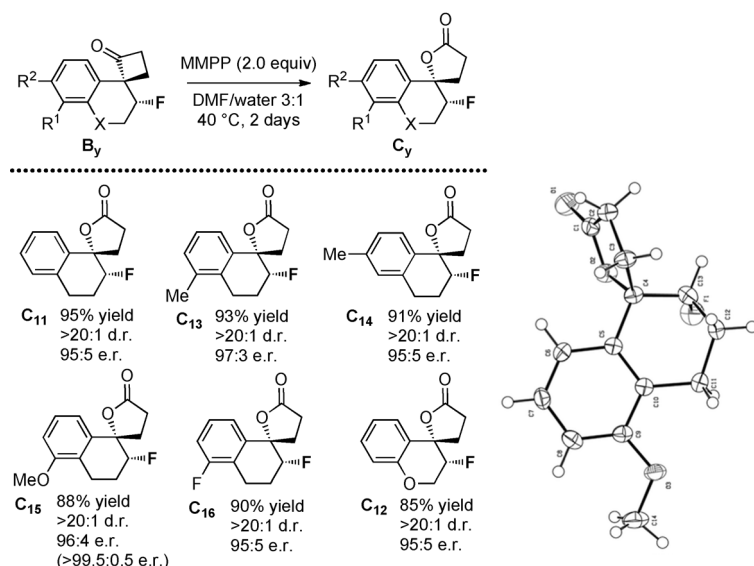
Scheme 5. A useful synthetic application of β-fluoro spiroketones and the X-ray crystal structure of C_{15}. The values in brackets show yields and enantiomer ratios after recrystallization. Thermal ellipsoids are set at 50% probability level. MMPP = magnesium mono-(peroxyphthalate).

absolute configurations (Scheme 5). X-ray diffractometry was employed to confirm the stereochemical course of this transformation. The overall two-step reaction sequence composed of 1) enantioselective fluorination/semi-pinacol rearrangement, followed by 2) stereospecific Baeyer–Villiger oxidation is synthetically relevant because it affords the products of a formal 5-exo-dig syn-fluorolactonization, a reaction that is unfeasible directly.

At this point, we were not satisfied with the observation that, while performing nicely for the strained allylic cyclopropanols and cyclobutanols, our fluorination-induced semi-pinacol reaction displayed a significant drop in enantioselectivity when switching to allylic cyclopentanols such as B_{19} (Scheme 1). Nevertheless, encouraged by the fact that even in this last reaction the chemical yield of the process remained high, we were interested in re-investigating the effect of 3,3'-bisaryl-di-substituted phosphoric acids $L_{1,4,5}$ and L_{9-11} on the stereoselectivity of the fluorination/semi-pinacol rearrangement of allylic cyclopentanols (Table 2).

As already seen before, during optimization studies with the cyclobutanol substrate A_1, bulky aryl groups at the 3,3'-posi-

tions of the BINOL-phosphoric acid are indispensible for high stereoselectivity in the fluorination/semi-pinacol reaction of the cyclopentanol substrate A_{19} as well. Simple phenyl groups as in acid L_1 and even the bulkier 1-anthracenyl substituents as in acid L_{10} did not suffice (Table 2, entries 1 and 5, respectively). When moving to the (R_a)-TRIP- or (R_a)-H_8-TRIP-derived phosphoric acids L_4 and L_9 a slight increase in both the diastereo- and enantioselectivity is observed, the diastereoselectivity being slightly higher for the latter acid (entries 2 and 4, respectively). Nevertheless, the real breakthrough came when the (R_a)-STRIP-derived phosphoric acid L_{11} (STRIP = 6,6'-bis(2,4,6-triissopropylphenyl)-1,1'-spirobiindan-7,7'-diyl hydrogenphosphate) was employed. Ligands based on the STRIP scaffold are notorious for their remarkably large bite angles.[26] In combination with Na_3PO_4 as base and in C_6H_5F/n-Hex 1:1 (v/v) as the solvent, catalyst L_{11} afforded the awaited β-fluoro spirocyclohexanone B_{19} in 77% isolated yield, 12:1 diastereomer and 90:10 enantiomer ratios (entry 6). It was later found out that switching from fluorobenzene to α,α,α-trifluorotoluene had a beneficial effect on yield and stereoselectivity, as did the replacement of n-hexane with n-heptane, which in turn allowed the reaction temperature to increase to −15°C. Under our final optimized reaction conditions, β-fluoro spiroketone B_{19} could be recovered as a single diastereomer and with 93:7 e.r. (entry 8).
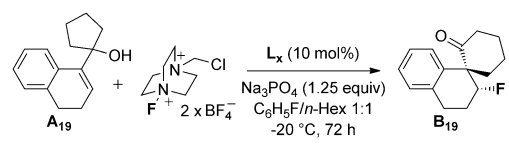
After having established the optimal reaction conditions for the fluorination-induced semi-pinacol rearrangement of allylic cyclopentanols, the generality of the procedure was investigated with a set of dihydronaphthalene- and chromene-based substrates ($J_{1-4,6}$ and J_5, respectively, see Scheme 6).

Once again, the relative and absolute configurations of products were unequivocally established by X-ray crystallography. Specifically, the structure of β-fluoro spirocyclohexanone B_{19} (= J_1) is shown in Scheme 6 above. As can be seen from the figure, the absolute stereochemistry comes from Re-face fluorination of the parent allylic cyclopentanol A_{19}. In comparison with the fluorination/semi-pinacol rearrangement reaction of allylic cyclopropanols and cyclobutanols, the same enantiomer is produced when a R_a-configured phosphate anion is used. On the other hand, the relative stereochemistry is the result of migration of the C—C bond that is anti with respect to the fluoronium bridge.

Diastereoselective reduction of the β-fluoro spiroketones was studied next. Such a transformation was interesting since it would lead to the formation of an extra stereogenic centre. Rather disappointingly, it was found out that common boron-based reducing agents like $NaBH_4$ or L-Selectride were not able to reduce spiroketone B_1 at low temperature (−78°C) over 24 h. To our great delight, however, treating substrate B_1 with Red-Al in toluene at −78°C led to complete reduction within 4 h. Furthermore, the recovered fluorinated alcohol I_1 was found to be diastereomerically pure (Scheme 7).

To probe the generality of diastereoselective reduction, three substrate β-fluoro spiroketones B_{14}, B_1 and B_{19} of three

↖↖ **These are not the final page numbers!**

Table 2. Re-visiting the fluorination-induced semi-pinacol rearrangement of allylic cyclopentanols.[a]

Entry	L_x	T [°C]	Base	Solvent	Yield [%][b]	d.r.[c]	e.r.[d]
1	L_1	−20	Na_3PO_4	PhF/cHex	71	3:2	69:31
2	L_4	−20	Na_3PO_4	PhF/nHex	90	9:1	87:13
3	L_5	−20	Na_3PO_4	PhF/nHex	53	4:1	84:16
4	L_9	−20	Na_3PO_4	PhF/nHex	92	10:1	87:13
5	L_{10}	−20	Na_3PO_4	PhF/nHex	74	3:2	76:24
6	L_{11}	−20	Na_3PO_4	PhF/nHex	77	12:1	90:10
7	L_{11}	−20	Na_3PO_4	$PhCF_3$/nHex	86	>20:1	91.5:8.5
8	L_{11}	−15	Na_3PO_4	$PhCF_3$/nHept	89	>20:1	93:7

[a] Reaction conditions: a solution of allylic alcohol A_{19} (0.20 mmol, 1.0 equiv), chiral phosphoric acid L_x (0.02 mmol, 10 mol%), powdered Selectfluor (0.30 mmol, 1.5 equiv), and powdered Na_3PO_4 (0.25 mmol, 1.25 equiv) in anhydrous C_6H_5F/nHex (1:1 v/v, total volume: 3.0 mL, 0.07 M) was stirred vigorously at −20 or −15 °C for 72 h. [b] Isolated yields after flash chromatography. [c] Determined by ^1H NMR spectroscopy of unpurified reaction mixtures. [d] Determined by chiral HPLC analysis of purified compounds. $PhCF_3 = \alpha,\alpha,\alpha$-trifluorotoluene. nHex = n-hexane. nHept = n-heptane.

different ring sizes (four-, five- and six-membered rings, respectively) were subjected to our previously optimized reaction conditions. In all three cases, very high diastereoselectivites of the corresponding fluorinated alcohols I_{14}, I_1 and I_{19} were observed. The relative configuration of products was tentatively assigned from homo- and heteronuclear Overhauser enhancement spectroscopy.[31,32]

Encouraged by our first results, we wondered whether an extension of the chiral counterion-directed enantioselective fluorination-initiated semi-pinacol rearrangement to the heavier halogen atoms (Br and I) would be feasible. As will be shown below, high enantioselectivities could indeed be maintained, but required the introduction of novel dicationic electrophilic halogen sources.

Of particular interest to us was the iodinative reaction, because iodinated hydrocarbons are notorious for their biological activity.[18] We began our studies with the reaction of allylic cyclobutanol A_1 with $(collidine)_2I^+PF_6^-$ (S_0) in methylene chloride at room temperature. To our great delight, the iodination/semi-pinacol reaction took place smoothly and afforded the expected β-iodo spiroketone D_1 as a single diastereomer and in 91% isolated yield (Scheme 8). Seeking for a suitable asymmetric PTC system, we repeated the above reaction in a less polar solvent (toluene) in presence of base and catalytic amounts of the lipophilic chiral phosphoric acid L_4 ((R_a)-TRIP). Disappointingly however, even though the reaction did proceed to completion, the recovered β-iodo spiroketone was racemic.[33]

Next, given the remarkable success of Selectfluor in anionic phase-transfer catalysis, we turned our attention to 1,4-diazobicyclo[2.2.2]octane (DABCO)-derived triply charged cations (S_{1-9}) as potential iodinating reagents (Scheme 8). Rather disappointingly, when employing S_1, the "exact" iodo analogue of Selectfluor, no reaction was observed under our previously established PTC conditions (toluene, Na_2CO_3, phosphoric acid L_4). This observation could be tentatively explained by the unfavoured predissociation equilibrium of S_1, generating insufficient amounts of the monoligated iodine(I) intermediate required for reactivity with alkenes.[28]

Consequently, switching to the bulkier and more lipophilic iodinating salts S_2 and S_3 turned out to be beneficial for reactivity. When combined with catalytic L_4 in toluene, both of these iodinating reagents afforded full conversion of A_1 to D_1, albeit with only insignificant levels of asymmetric induction (ca. 60:40 e.r.).

We speculated that one possible rationalization for the low enantiomeric ratios observed with our PTC system gravitated around the olefin-to-olefin halogen exchange problem, known to occur between the transient bromiranium/iodiranium cations and leading to product racemization.[29] Variable-temperature NMR studies by Brown and co-workers have shown that a fast and degenerate olefin-to-olefin transfer occurs between adamantylidene adamantane and the bromonium ion derived from it.[29b] This process is assumed to take place through a low-barrier associative displacement at the halogen atom (Scheme 9).

In an attempt to solve for this problem, we were intrigued by the possibility of further exploring the steric and electronic parameters of the nitrogen substituent (R) of the iodinating reagent (Scheme 8). Following the logic of increasing the lipophilicity, further fluorination of the benzene ring of the R substituent afforded a more active reagent (S_4), but the enantiomer ratio remained unacceptably low (64:36 e.r.). Replacing the benzene ring with the bulkier 9-anthracenyl substituent (S_5) led to a concomitant drop in yield and in stereoselectivity. Gratifyingly, switching to the more sterically demanding 2,4,6-tris(isopropyl)phenyl substituent (S_6) improved the enantiomeric ratio markedly (85:15 e.r.). A similar effect was obtained when employing the branched benzhydryl-based substituents (S_8 and S_9, both 86:14 e.r.). Of note, further increasing the size of the R substituent by using the 2,4,6-tris(cyclopentyl)phenyl group (S_7) instead of the 2,4,6-tris(isopropyl)phenyl one completely inhibited the reactivity. Encouraged by these prelimina-
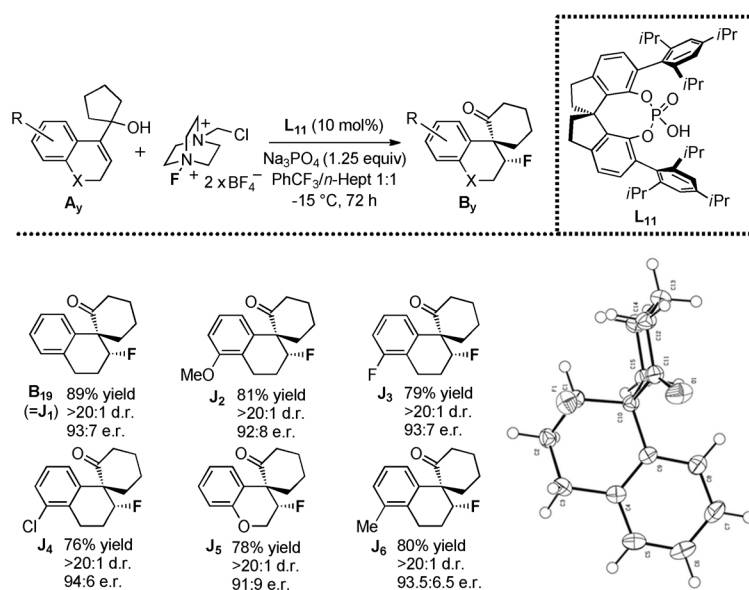
Scheme 6. Substrate scope for the fluorination-induced semi-pinacol rearrangement of allylic cyclopentanols and the X-ray crystal structure of B_{19}. Thermal ellipsoids are set at 50% probability level.
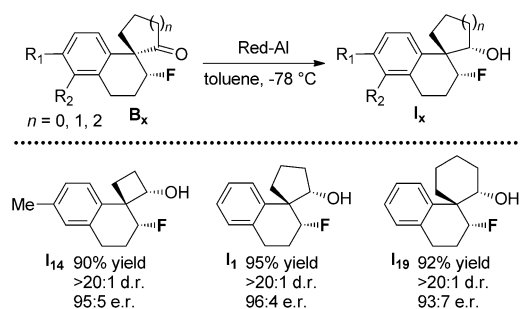
Scheme 7. Diastereoselective reduction of β-fluoro spiroketones.

ry results, we selected the iodinating reagent S_9 for further optimization studies.

After having selected iodinating reagent S_9 as the optimal one the solvent, the base, as well as the structure of the chiral phosphate anion were investigated next, in an attempt to improve the enantioselectivity of the iodination/semi-pinacol reaction (Table 3).

A quick overview of the synthetically accessible enantiopure phosphoric acids L_{1-11}, using toluene as the solvent and Na_2CO_3 as the base, revealed L_9 as the optimal one (Table 3, entry 9). Changing the base from Na_2CO_3 to Na_3PO_4 improved the enantiomeric ratio from 87:13 to 89:11, accordingly (entry 12). Fluorinated aromatic solvents like PhF or $PhCF_3$ led to quasi-racemic product mixtures (entries 13, 14). Including n-hexane into a binary solvent mixture with toluene, which proved to be beneficial for the related fluorination/semi-pinacol transposition, did not increase the enantiomeric excess in the present iodination/semi-pinacol reaction sequence (entry 18). Neither did the switch to the less polar *para*-xylene solvent (entry 15). Gratifyingly, when carrying out the reaction in ethylbenzene as the solvent, an important increase of the selectivity was observed (91:9 e.r.). Further adjustments, includ-

ing dilution of the reaction medium to 0.05 M, coupled with extension of the reaction time to 72 h, afforded the optimal conditions for the title transformation (entry 20).

The DABCO-derived triply charged cationic iodinating reagents (S_{1-9}) were readily synthesized using experimental procedures adapted from the literature.[14b] To this end, DABCO (5) was first mono-alkylated with the appropriate primary benzylic chloride to furnish mono-quaternary ammonium salts (6) (Scheme 10). These salts were then subjected to anion metathesis, followed by coordination to iodine(I). The resultant highly insoluble, triply charged iodinating reagents S_{1-7} were isolated by precipitation, and subsequently purified by re-precipitation from nitromethane.

The benzhydryl-substituted iodinating reagents S_{8-10} were prepared in an analogous manner (Scheme 11). The sole complication arose from the poor reactivity of benzhydryl chlorides towards alkylation by DABCO. The problem was solved by switching to the more reactive benzhydryl bromides 9, which were in turn prepared from the corresponding aryls 8 through dimerization followed by deoxygenative bromination.

With the optimal reaction conditions being established, the substrate scope of our newly developed iodination-initiated Wagner–Meerwein rearrangement was investigated. To this end, strained allylic alcohols A_{1-25} were reacted with iodinating reagent S_9 and catalytic amounts of enantiopure phosphoric acid L_9 under biphasic Na_3PO_4/ethylbenzene conditions. The results are summarized in Scheme 12 below.

Both, three- ($n = 0$, products D_{13-21}) and four-membered ($n = 1$, products D_{1-12}) allylic alcohols were amenable to enantioselective iodination/ring-expansion reaction sequence, which occurred equally well with scaffolds based on dihydronaphthalene (X = CH_2, for example, D_1), chromene (X = O, for example, D_8), indene (X = n/a, for example, D_{12}) and dihydrobenzoazulene (X = CH_2CH_2, product D_{25}) ring systems. A distinct feature of the iodination reaction is its high tolerance towards substitution at positions C5 (e.g. product D_4), C6 (e.g. product D_{22}) and C7 (e.g. product D_{24}) of the phenyl ring. A much narrower substitution tolerance was observed for the fluorination reaction. The title enantioselective transformation was also less sensitive to substituent electronic effects when compared to the previously reported fluorination analogue. These marked deviations of substrate tolerance between the fluoro- and iodo-initiated transpositions constitute a hint at the mechanistic dichotomy that likely exists for these two reactions.

When switching to the bromination/semi-pinacol reaction, it was quickly established that the bulky 2,4,6-tris(isopropyl)-phenyl-substituted DABCO-derived brominating reagent R_6, an exact analogue of the previously described iodinating reagent S_6, was capable of conducting a highly enantioselective halogenation of substrate A_1 under very similar reaction conditions (chiral phosphoric acid L_9, Na_3PO_4 as base, and ethylbenzene as solvent).
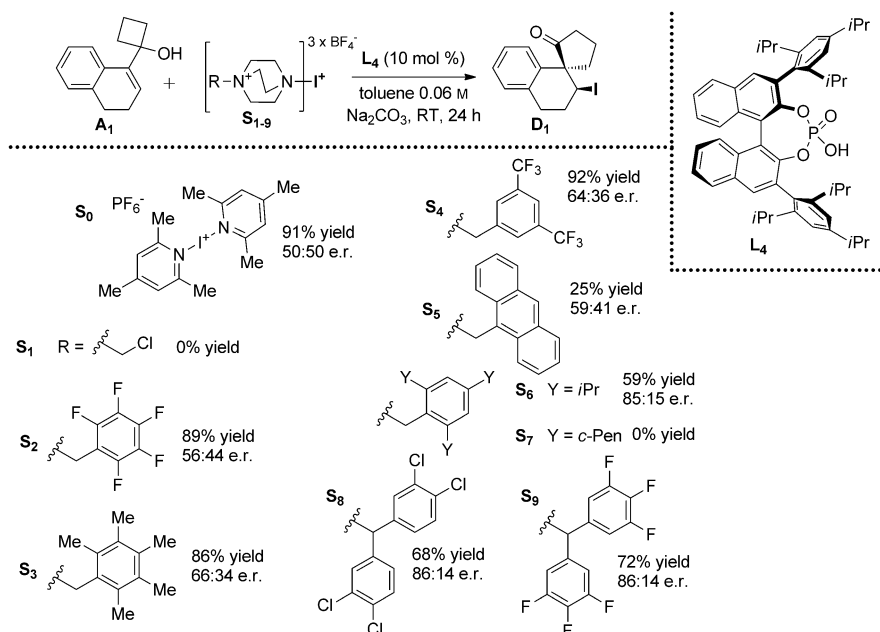
Scheme 8. Optimization of the iodinating reagent S_{1-9}.
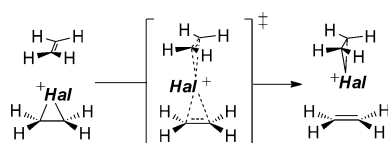
Scheme 9. Mechanism of the olefin-to-olefin halogen exchange that leads to deterioration of enantiomeric excess. Hal = Br, I.

The bromination-initiated semi-pinacol rearrangement reaction proved to be remarkably general in terms of the substrate scope (Scheme 13). More specifically, three- ($n = 0$, products F_{17} and F_{20}) and four-membered ($n = 1$, products $F_{1,2,8,12}$ and F_{27}) allylic alcohols were amenable to enantioselective catalysis, which occurred equally well with scaffolds based on dihydronaphthalene ($X = CH_2$, products $F_{1,2,17}$), chromene ($X = O$, products F_8 and F_{20}), indene ($X = n/a$, product F_{12}) and dihydrobenzoazulene ($X = CH_2CH_2$, product F_{27}) ring systems. It is important to note that the enantiomer ratios of the recovered β-bromo spiroketones F_y were invariably higher than those obtained for their β-iodo counterparts D_y.

Single crystals of β-iodo spiroketone D_8 and β-bromo spiroketone F_2 were grown for X-ray diffraction analysis (Scheme 14).

It is fascinating to note that, for an identically configured enantiopure phosphoric acid, the sense of absolute induction is opposite to that observed for the related fluorination-initiated Wagner–Meerwein rearrangement (*Si*-face halogenation for the former, whereas *Re*-face halogenation for the latter). Consequently, *Si*-face halogenation seems to be a prerogative of the heavier halogens (Br, I) that pass through cyclic haliranium ions, whereas *Re*-face halogenation is limited to fluorine that is notorious for not forming cyclic haliranium ions. On the other

hand, the relative configuration was consistent with selective migration of the C—C bond that is *anti* to the iodonium bridge.
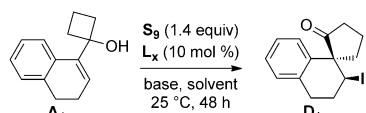
Very importantly, the hereby-described bromination- and iodination-initiated semi-pinacol rearrangements were readily amenable to scale-up. As one example, allylic alcohol A_8 was converted into the corresponding β-iodo spiroketone D_8 in excellent yield and without a drop in the enantioselectivity (Scheme 15). Furthermore, two product β-iodo spiroketones (D_8 and D_9) were subjected to an S_N2 reaction with sodium azide. Under optimized experimental conditions, the substitution reaction took place stereospecifically (clean inversion) and without enantioerosion, and 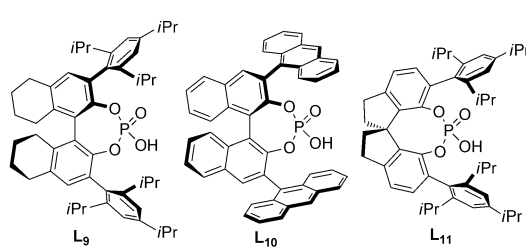the corresponding azides $E_{8,9}$ were recovered in high isolated yields. The described derivatization by an S_N2 reaction serves as a demonstration of the synthetic utility of product β-iodo spiroketones, giving rise to products inaccessible directly from a semi-pinacol rearrangement. Moreover, organic azides are very versatile, energy-rich intermediates that have recently enjoyed considerable interest in the synthetic community.[30]

Eager to further expand the limits of our halogenative semi-pinacol rearrangement methodology, we were interested in applying the biphasic catalytic system to substrates prone to desymmetrization (K_x). If successful, these reactions would further increase the synthetic utility of the process by incorporating an additional stereogenic centre into the products. To probe our strategy, two substrates belonging to the C_S point group of symmetry were chosen: one based on the dihydropyrane (K_1) and the other based on the dihydronaphthalene (K_2) skeletons (Scheme 16).
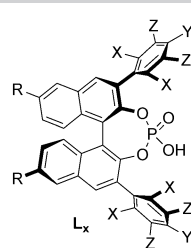
To our great delight, desymmetrized products (M_x, N_x) were obtained in high yields, high diastereoselectivities and with encouraging enantioselectivities (up to 95:5 e.r.) when using reaction conditions previously optimized for the fluorination- and bromination-initiated semi-pinacol reactions. Remarkably, the level of asymmetric induction for substrate K_1 was considerably improved when compared to the simpler substrate A_{26}, also based on the dihydropyran skeleton. These preliminary results demonstrate the outstanding ability of our methodology to bring stereochemical complexity into molecules in few synthetic steps. Our recent advances in this field, involving the extension of the fluorination/semi-pinacol methodology to ring-expansion of cyclopropylamines,[39] as well as a stereodivergent reaction on the racemic mixture,[27] are beyond the scope of the present Full Paper and will not be described in further detail. It is also important to note here that all our attempts to

Table 3. Optimization of the reaction conditions for the iodination-initiated semi-pinacol rearrangement.

Entry	L_x	Base	Solvent	Yield [%][b]	d.r.[c]	e.r.[d]
1	L_1	Na_2CO_3	PhMe	64	>20:1	59:41
2	L_2	Na_2CO_3	PhMe	8	>20:1	n.d.
3	L_3	Na_2CO_3	PhMe	78	>20:1	54:46
4	L_4	Na_2CO_3	PhMe	68	>20:1	86:14
5	L_5	Na_2CO_3	PhMe	0	>20:1	n.d.
6	L_6	Na_2CO_3	PhMe	22	>20:1	87:13
7	L_7	Na_2CO_3	PhMe	66	>20:1	82:18
8	L_8	Na_2CO_3	PhMe	67	>20:1	79:21
9	L_9	Na_2CO_3	PhMe	73	>20:1	87:13
10	L_{10}	Na_2CO_3	PhMe	52	>20:1	66:34
11	L_{11}	Na_2CO_3	PhMe	60	>20:1	37:63[e]
12	L_9	Na_3PO_4	PhMe	76	>20:1	89:11
13	L_9	Na_3PO_4	PhF	86	>20:1	53:47
14	L_9	Na_3PO_4	$PhCF_3$	88	>20:1	52:48
15	L_9	Na_3PO_4	p-Xyl	74	>20:1	88:12
16	L_9	Na_3PO_4	PhH	79	>20:1	84:16
17	L_9	Na_3PO_4	$(iPr)_2O$	82	>20:1	85:15
18	L_9	Na_3PO_4	PhMe/nHex	70	>20:1	87:13
19	L_9	Na_3PO_4	PhEt	85	>20:1	91:9
20[f]	L_9	Na_3PO_4	PhEt	87	>20:1	93:7

[a] Reaction conditions: a solution of allylic alcohol A_1 (0.20 mmol, 1.0 equiv), chiral phosphoric acid L_x (0.02 mmol, 10 mol%), iodinating reagent S_9 (0.28 mmol, 1.4 equiv), and powdered base (0.80 mmol, 4.0 equiv) in anhydrous solvent (3.0 mL, 0.07 M) was stirred vigorously at 25 °C for 48 h. [b] Isolated yields after flash chromatography. [c] Determined by ^1H NMR spectroscopy of unpurified reaction mixtures. [d] Determined by chiral HPLC of purified compounds. [e] The opposite enantiomer was obtained. [f] Molar concentration decreased to 0.05 M, reaction time increased to 72 h, S_9 reduced to 1.3 equiv p-Xyl = para-xylene. nHex = n-hexane. n.d. = not determined.

Scheme 10. Synthesis of the tricationic iodinating reagents S_{1-7}.

extend our asymmetric phase-transfer methodology to the chlorination-initiated semi-pinacol rearrangement failed, presumably due to decomposition of the corresponding cationic chlorinating reagents.

Mechanistic Aspects

After having discovered that the fluorination-initiated semi-pinacol rearrangement of allylic alcohols of at least three classes (cyclopropanols, cyclobutanols and cyclopentanols) can be rendered enantioselective by ion-pairing the intermediate fluoronium cation with a chiral enantiopure phosphate anion, we were eager to find out whether mechanistic studies could shed light onto the origins of the high enantioselectivities observed in these reactions.

The initial goal of our mechanistic studies was to determine an experimental rate law for the fluorination-initiated semi-pinacol rearrangement reaction.

At first glance, the fluorination-initiated semi-pinacol rearrangement seemed to be a rather complex reaction (Scheme 17). To simplify things somewhat, the overall reaction was mentally partitioned into two key events, each of which takes place at a different physical location in the reaction vessel. The first event takes place at the interface between the solid phase (containing Selectfluor and Na_3PO_4) and the liquid phase (containing the reactant **1** and the product **3**) and itself involves two interfacial processes: 1) deprotonation of the phosphoric acid pre-catalyst (PA—H) by the inorganic base (Na_3PO_4) and concomitant generation of the lipophilic phosphate anion PA⁻, and 2) extraction of the insoluble Selectfluor cation into the liquid phase and formation of the reactive lipophilic ion pair **2**. Between these two processes, the former can be described by an acid–base equilibrium constant (K_{eq}), while the latter by a rate constant of extraction (k_{ext}).
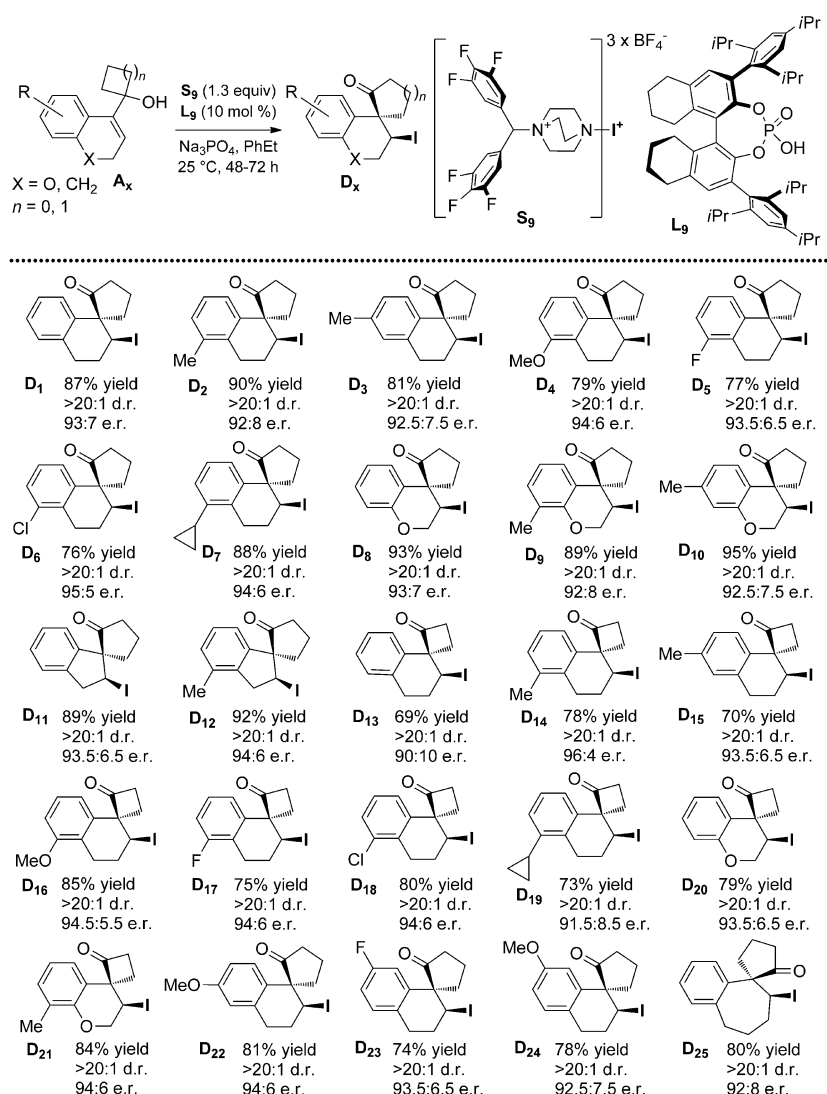
The second event involves the actual fluorination/semi-pinacol rearrangement reaction that takes place entirely in the liquid phase, and combines the sub-

↖↖ These are not the final page numbers!
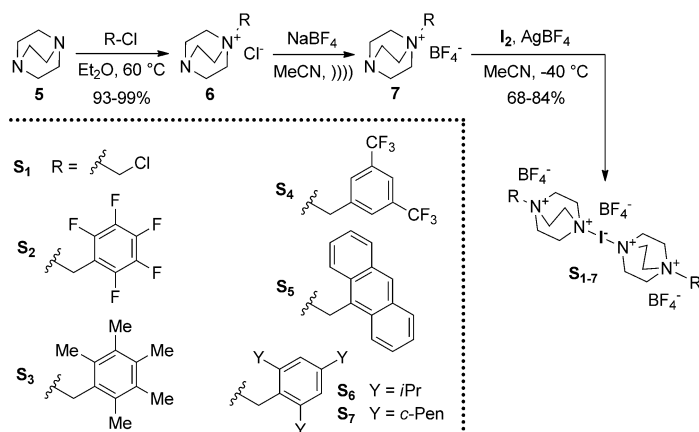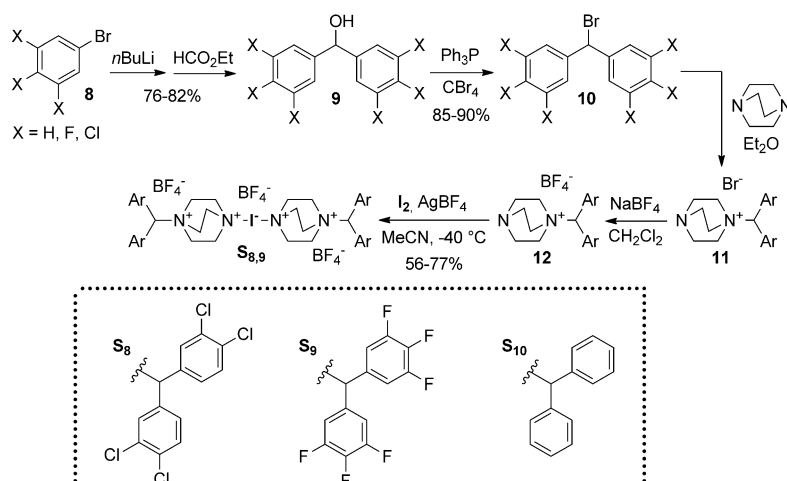
Scheme 11. Synthesis of the benzhydryl-substituted tricationic iodinating reagents S$_{8-10}$.

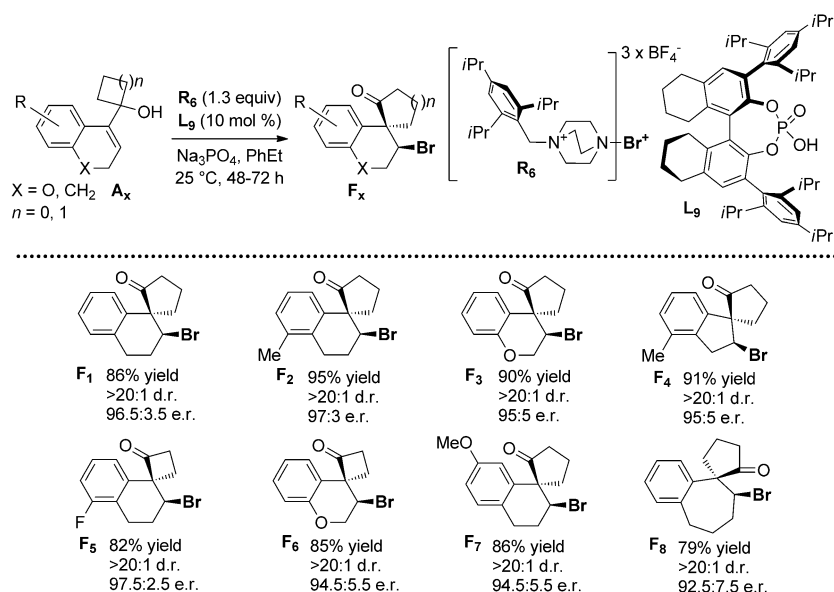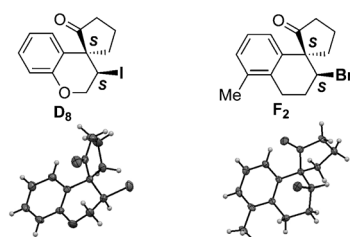**Scheme 12.** Substrate scope of the iodination/semi-pinacol rearrangement reaction.

the homogeneous chemical reaction involves two elementary steps that share a common intermediate **4**, which can take the form of either a fluoronium-bridged species, a protonated epoxide, or a β-fluoro benzylic carbocation (or a mixture of any of these three extremes). The first elementary reaction is a bimolecular collision between **1** and **2** and we expect it to be second order. The second elementary reaction involves a unimolecular rearrangement of intermediate **4** that leads to product **3** and we expect it to be first order.

It is clear that both of the two interfacial processes involved (deprotonation of PA–H and extraction of Selectfluor) must be kinetically complex. However, in the limiting case in which the rates of these interfacial processes are significantly higher than the rates of the chemical reaction, precisely $K_{eq}, k_{ext} \gg k_1, k_2$ we expect the concentration of the reactive lipophilic ion pair **2** to stay small and constant during the reaction. Consequently, we could apply the steady-state approximation (SSA) to describe the concentration of **2**, which would in turn lead to overall pseudo-first order kinetics of the product formation. Due to the very high dissociation energy of the C–F bond (ca. 110 kcal mol^{-1}), we assume that the first step of the chemical reaction (the electrophilic fluorination of the C=C double bond) is essentially irreversible. Furthermore, since the intermediate carbocation **4** is a high-energy reaction intermediate, its unimolecular decomposition to product **3** must be a rapid process.

In the other extreme, if the chemical reaction under study is faster than the interfacial processes, that is, $k_1, k_2 \gg K_{eq}, k_{ext}$, then we expect complex overall kinetics of product formation that are dominated by interfacial phenomena (Scheme 18). Finally, in the third scenario, we

strate allylic alcohol **1** with the reactive lipophilic ion-pair **2** to yield the product β-fluoro spiroketone **3**. Thus, we can see that

Scheme 13. Substrate scope of the bromination/semi-pinacol rearrangement reaction.

Scheme 14. Relative and absolute configurations of β-iodo spiroketone **D₈** and β-bromo spiroketone **F₂**, as determined by X-ray crystallography. Thermal ellipsoids are set at 50% probability level.
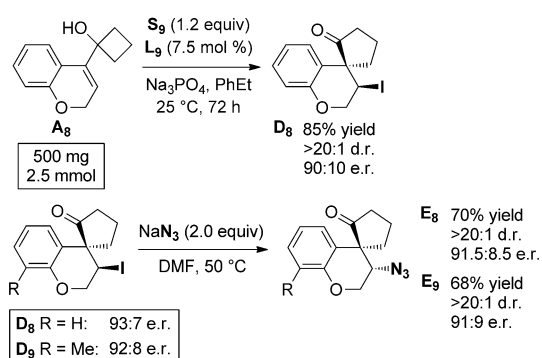
Scheme 15. Scale up of the catalytic enantioselective iodination-initiated semi-pinacol rearrangement (top), and a stereospecific derivatization of the product β-iodo spiroketones **D₈** and **D₉** (bottom).

thought to alleviate the problems related to complex interfacial behaviour by carrying out the fluorination/semi-pinacol reaction under homogeneous and stoichiometric conditions. Precisely, the use of stoichiometric amounts of preformed reactive lipophilic ion pair **2** would allow switching to monophasic re-

action conditions and reducing the kinetic expressions to simple second-order behaviour.

The initial in situ FTIR experiments were performed under heterogeneous phase-transfer conditions. However, the obtained (concentration, time) recordings were essentially linear and not conclusive. Presumably, slow interfacial processes dominated the kinetics of formation of **3**. Matters were further complicated by the presence of an inhomogeneous solution layer adjacent to the IR window, which lead to broadening of the absorption bands. Consequently, the homogeneous stoichiometric approach was chosen for further studies, as it alleviated both of the above limitations.

Prior to carrying out kinetic experiments, the validity of the stoichiometric approach was established by: 1) preparing the reactive lipophilic ion pair **2** by anion metathesis at $T_2 = -8\,°C$, 2) filtering off the NaBF₄ salts, and 3) subjecting substrate **1** to reaction with a stoichiometric amount of **2** under homogeneous conditions (Scheme 19). As can be seen from the scheme, the level of stereoinduction in the product **3**, obtained with our stoichiometric protocol, is identical to that observed under conventional PTC conditions with phosphoric acid **L₄** (compare with entry 3 in Table 3). Furthermore, the reaction time was considerably reduced (around 8 h) when compared to the PTC protocol (typically 72 h). Additionally, the ¹H NMR spectrum of **2** clearly indicates the incorporation of two **L₄** phosphates for one Selectfluor dication.[32] The slight deterioration of the chemical yield of **3** under stoichiometric reaction conditions can be explained by partial decomposition of the ion pair **2** in the course of the filtration step. A marked improvement of the isolated yield was obtained when employing the lipophilic ion pair **2** prepared in situ and used without filtration.

To decipher the rate law of the fluorination-induced semi-pinacol reaction, we have chosen the approach developed by Blackmond for reaction progress kinetic analysis.[34] The sole deviation from the original protocol was the fact that we have adapted the graphical tools developed to study catalytic reactions for our process performed under stoichiometric conditions.

The progress of the reaction was continuously followed over the entire course by in-situ FTIR absorption measurements at temperature $T_2 = -8\,°C$ (265 K). Initially, the IR-intensity (I_{IR}) of the C–F bond-stretching band (around ca. 1066 cm⁻¹) was correlated to the concentration of product **3** by calibrating the in situ measurement. In turn, calibration was achieved by periodic sampling of the reaction mixture and assessing the concentrations of species **1** and **3** by ¹H NMR spectroscopy in the pres-
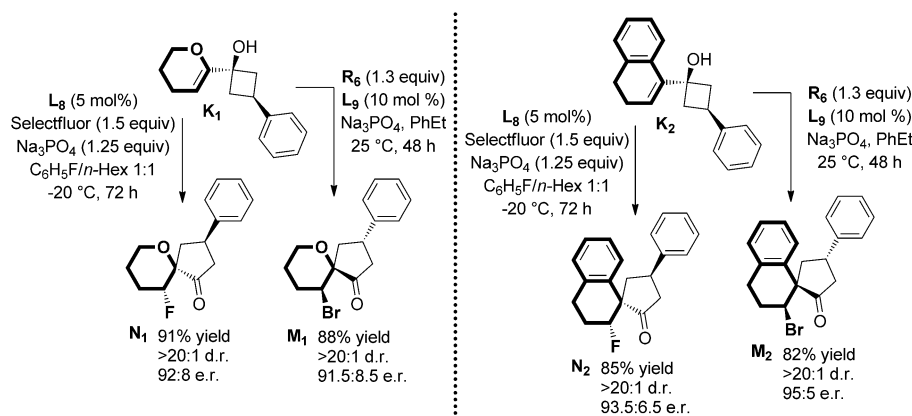
Scheme 16. Desymmetrization of C_S-symmetric substrates (**K_x**) through halogenation-initiated semi-pinacol rearrangement.

ence of an internal standard (1,3,5-trimethoxybenzene, molar concentration in the NMR tube: 50 mM). A good overlay between the two measurements indicated that the IR intensity at 1066 cm^{-1} indeed correlated well with the turnover of substrate molecules into the product (Figure 5).

The time intervals at which NMR sampling was made are (from left to right on Figure 5): 15, 115, 140, 145, 180, and 270 min. The corresponding molar concentrations of β-fluoro
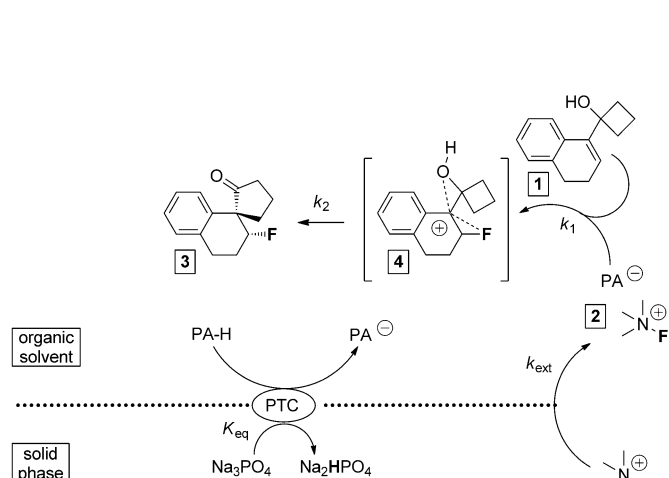
Scheme 17. Dissection of the fluorination/semi-pinacol reaction mechanism into elementary steps. PTC = phase-transfer catalyst. PA = phosphoric acid.
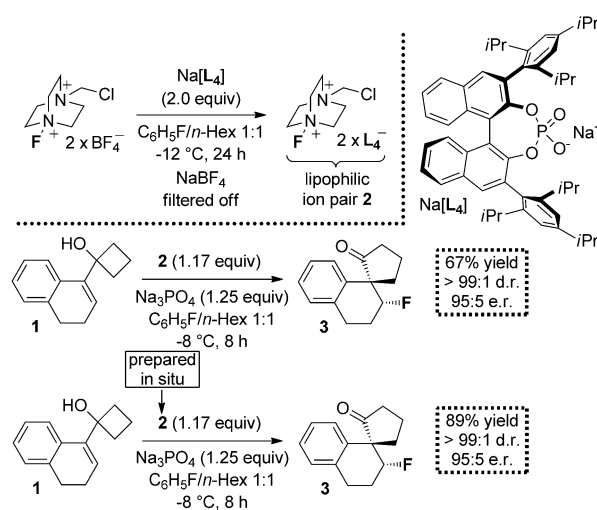
Scheme 19. Validation of the stoichiometric approach.
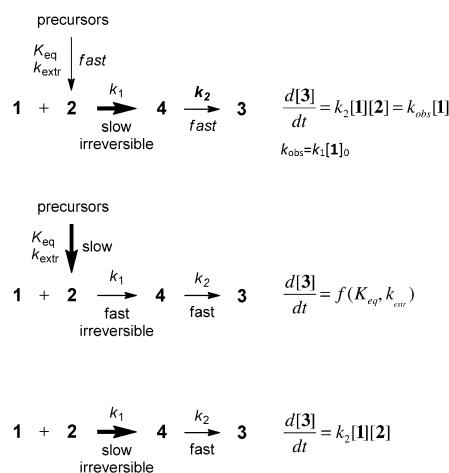
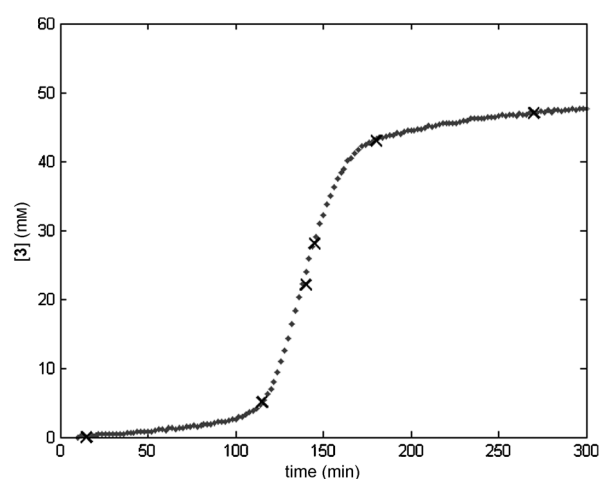**Scheme 18.** Three limiting kinetic scenarios for the fluorination/semi-pinacol reaction.

Figure 5. Molar concentration of **3** versus time for the reaction shown in Scheme 19, as monitored by in situ FTIR (grey dots) and verified by ^{1}H NMR spectroscopic analysis (black crosses). $T_2 = 265$ K. $[\mathbf{1}]_0 = 50$ mM. ["excess"] = 23.4 mM.

These are not the final page numbers! ↗↗

spiroketone **3** (as determined by ^{1}H NMR spectroscopic analysis) being: 0, 5, 22, 28, 43, and 47 mM. ^{1}H NMR spectra of aliquots (sample size: 500 μL) were recorded after filtration of the crude sample through a short plug of silica gel (for the removal of residual **2**) and addition of 1,3,5-trimethoxybenzene (internal standard) of known molar concentration in the NMR tube (50 mM).[32] All peaks were then integrated with normalization with respect to the two reference peaks of 1,3,5-trimethoxybenzene (at $\delta = 6.09$ and 3.77 ppm).

The calibration experiment described above delineated our "standard" reaction conditions used as the reference point for all of the subsequent kinetic experiments (Scheme 20). Precise-
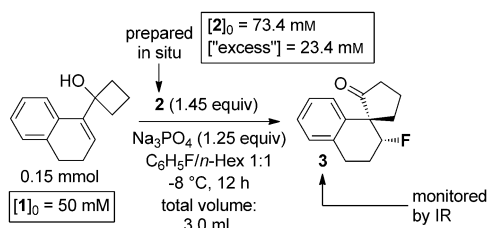
Scheme 20. "Standard" reaction conditions used for kinetic experiments.

ly, under this set of reaction conditions, the molar concentration profile of product **3** follows a sigmoidal-shaped curve that reaches a plateau of 50 mM in about 5 h, when the reaction is essentially complete (as checked by ^{1}H NMR spectroscopy).

Although concentrations [**1**] and [**2**] both change with time, their values can be predicted because the manner in which they change is linked to the reaction stoichiometry. For the reaction shown in Scheme 20, the stoichiometry dictates that each time one molecule of substrate **1** is converted into one molecule of product **3**, one molecule of lipophilic ion pair **2** is necessarily also converted. We define a parameter called the ["excess"], which is equal to the difference in the initial concentrations of the two substrates [Eq. (1)].

$$1 + 2 \xrightarrow{k_1} [4] \xrightarrow{k_2} 3$$

$$\frac{d[3]_t}{dt} = k_1[1]_t[2]_t$$
$$[3]_t = const \times I_{IR}$$
$$[1]_t = [1]_0 - [3]_t \qquad (1)$$
$$[2]_t = [1]_t + [2]_0 - [1]_0 = [1]_t + ["excess"]$$

The analytical expressions for concentrations [**1**] and [**2**] as a function of [**3**] that are given in Equation (1) above can be used to trace the molar concentration profiles of species **1** and **2** (Figure 6). Graphically, the value of ["excess"] can be determined as the difference in plateau heights of the corresponding (concentration, time) plots. Thus, for our "standard" conditions this value stands at 23.4 mM, which corresponds to 1.45 equivalents of the lipophilic ion pair **2** with respect to substrate **1**.

With a set of calibrated (concentration, time) plots describing the reaction progression in hand, we then employed the
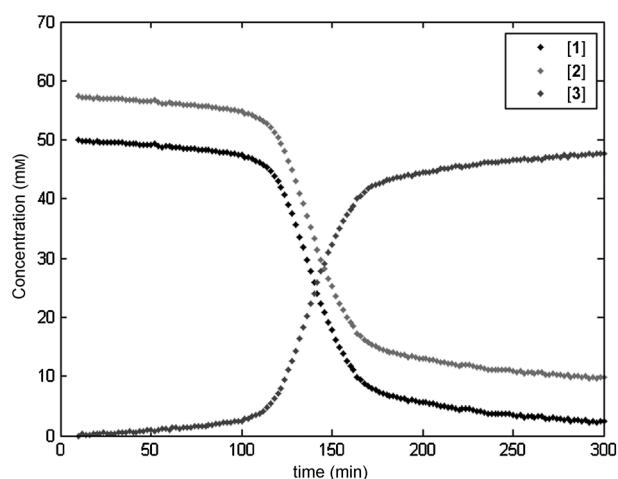

Figure 6. Molar concentration profiles of the reaction components **1** (black), **2** (light grey) and **3** (dark grey) under the "standard" reaction conditions. $T_2 = 265$ K. $[1]_0 = 50$ mM. ["excess"] = 23.4 mM.

graphical tools provided by Blackmond et al.[34] to draw conclusions regarding the kinetic orders of reactants **1** and **2**. To this end, a plot of rate versus time had to be obtained (the differential measurement). Because we did not have access to a differential measurement technique (e.g. calorimetry), the reaction rate had to be calculated from the (concentration, time) data set (the integral measurement) by fitting the data to an appropriate Smoothing Spline function, and then differentiating this function to obtain the (rate, time) data (Figure 7).
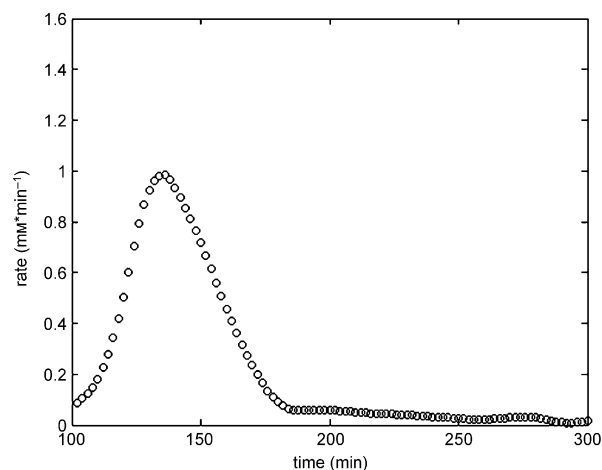

Figure 7. Differential measurement data (reaction rate), obtained by processing of the integral measurement data. $T_2 = 265$ K. $[1]_0 = 50$ mM. ["excess"] = 23.4 mM.

Graphically, we can see that the fluorination/semi-pinacol reaction displays a marked induction period during which the rate rises. After about 2.5 h, the reaction rate reaches its maximum, before slowly dropping back down to zero. It is during this rather short descent period that the reaction is in the steady-state mode and its behaviour can be quantified.

Next, the differential measurement was plotted as the *y*-axis and the integral measurement as the *x*-axis, thus leaving time out of the picture. The resultant bell-shaped curve, termed the "graphical rate equation", was used as a graphical imprint of the reaction kinetics under a given set of initial conditions (Figure 8). Note that, in contrast to Figure 7, the rate decreases when moving from the right to the left side of the plot (as the concentration of **1** decreases).
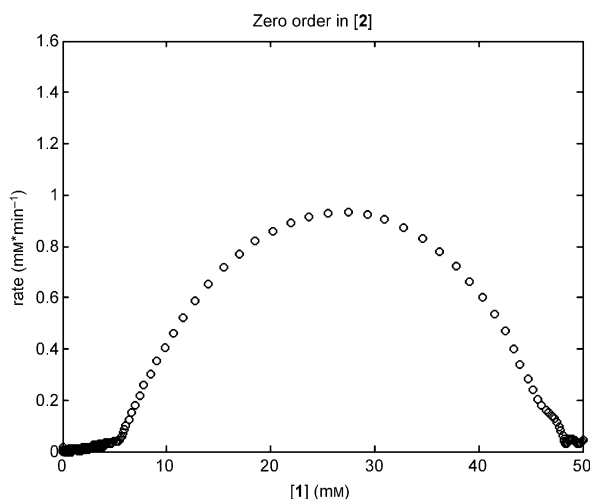

Figure 8. Graphical rate equation for the reaction shown in Scheme 20. $T_2 = 265$ K. $[1]_0 = 50$ mm. ["excess"] = 23.4 mm.

A second kinetic profile was recorded for a reaction with the same ["excess"] value but a different starting concentration of **1**. This is equivalent to carrying out the same experiment from two different starting points and, in catalytic reactions, it is usually performed to probe for complexities such as product inhibition or catalyst deactivation. Two plots with two graphical rate equations each, with the same ["excess"] value (left: 23.4 mm, right: 12.3 mm) but a different $[1]_0$ (left and right, both: 50 mm and 66.7 mm) are given in Figure 9 below. An overlay between the two plots can be observed in the vicinity of the steady-state concentration regime (low concentration of **1**).

A set of kinetic experiments employing different ["excess"] values but an identical $[1]_0$ was carried out next. The aim of these experiments was to determine the kinetic orders of reactants **1** and **2**. Figure 10 below presents the graphical rate equations for these three experiments.

The absence of overlays between the three plots signifies that the reaction under study is not zero order in **2**. To probe whether the reaction is first order in **1**, plots of rate/[1] versus [2] for experiments with different ["excess"] values but an identical $[1]_0$ value were created (Figure 11).

An overlay between these plots in the vicinity of the steady-state concentration regime indicates that the fluorination/semi-pinacol reaction is first order in **1**. Furthermore, the second-order rate constant can be extracted from the linear part of the plot. More specifically, the mean value at tempera-
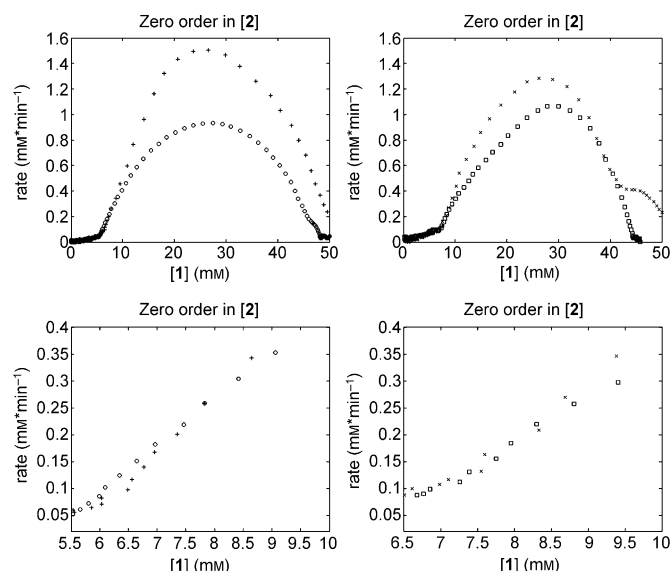

Figure 9. Two plots with two graphical rate equations each, for experiments with an identical ["excess"] value (left: 23.4 mm, right: 12.3 mm) but different starting concentrations of **1** (left and right, both: 50 and 66.7 mm). A caption of the steady-state concentration regime is also given to see the overlap. Black circles: $[1]_0 = 50$ mm, ["excess"] = 23.4 mm; black pluses: $[1]_0 = 66.7$ mm, ["excess"] = 23.4 mm; black squares: $[1]_0 = 50$ mm, ["excess"] = 12.3 mm; grey crosses: $[1]_0 = 66.7$ mm, ["excess"] = 12.3 mm.
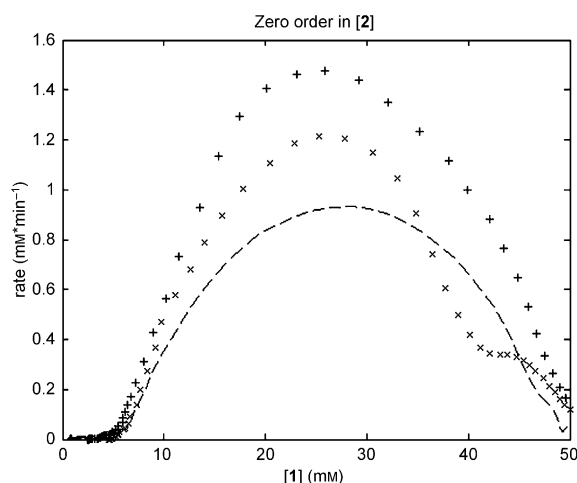

Figure 10. Three graphical rate equations for experiments with different ["excess"] values, recorded at temperature $T_2 = -8\,^\circ$C. Black short lines: ["excess"] = 7.4 mm; grey crosses: ["excess"] = 12.3 mm; black pluses: ["excess"] = 23.4 mm. $[1]_0 = 50$ mm.

ture $T_2 = -8\,^\circ$C being: $k_{obs}(T_2) = 0.125$ m^{-1} s^{-1}. The confidence interval for this value being: 0.015 m^{-1} s^{-1}.

An analogical procedure, involving an overlay between plots of rate/[2] versus [1], indicated that the reaction under study was first order in **2** as well (Figure 12).

Additionally, the second-order rate constant can be extracted from the linear part of this plot as well. More specifically, the mean value at temperature $T_2 = -8\,^\circ$C being: $k_{obs}(T_2) = 0.078$ m^{-1} s^{-1}. The confidence interval for this value being:

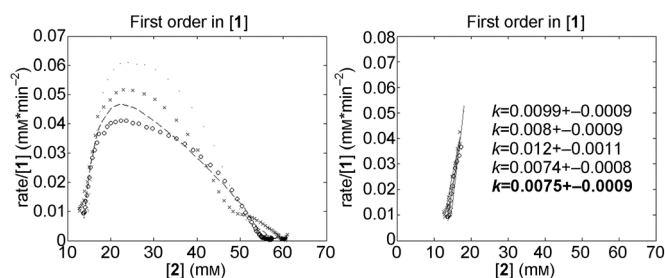**These are not the final page numbers!** ↗↗

Figure 11. Probing for first order in 1 (left). Black circles: ["excess"] = 23.4 mM; black short lines: ["excess"] = 7.4 mM; grey crosses: ["excess"] = 12.3 mM; black dots: ["excess"] = 26.7 mM. Graphical estimation of the second-order rate constant (right). The slope has the units of $mM^{-1}min^{-1}$. The mean value is given in black.

In the right plot:
$k=0.0099+-0.0009$
$k=0.008+-0.0009$
$k=0.012+-0.0011$
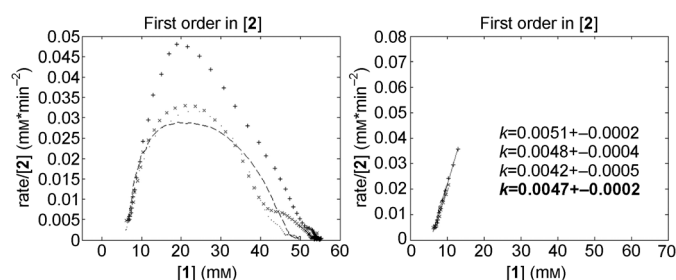$k=0.0074+-0.0008$
$k=0.0075+-0.0009$

Figure 12. Probing for first order in 2 (left). Black short lines: ["excess"] = 7.4 mM; black dots: ["excess"] = 26.7 mM; grey crosses: ["excess"] = 12.3 mM; black pluses: ["excess"] = 23.4 mM. Graphical estimation of the second-order rate constant (right). The slope has the units of $mM^{-1}min^{-1}$. The mean value is given in black.

In the right plot:
$k=0.0051+-0.0002$
$k=0.0048+-0.0004$
$k=0.0042+-0.0005$
$k=0.0047+-0.0002$

0.003 $M^{-1}s^{-1}$. Now, taking the average from the values obtained with plots on Figures 11 and , gives us the following (final) result: $k_{obs}(T_2) = 0.101\ M^{-1}s^{-1}$.

In conclusion to our kinetic study, we have shown by using a graphical approach that our fluorination/semi-pinacol reaction is overall second order, first order with respect to each reactant 1 and 2 [Eq. (2)].

$$rate = k_{obs}[1][2] \tag{2}$$

All the graphical manipulations described above were carried out at a single reaction temperature, defined in the "standard" conditions ($T_2 = -8\,°C$, 265 K). By repeating these manipulations with (concentration, time) data sets collected at three other temperature points ($T_1 = +2$, $T_2 = -8$, $T_3 = -20$, $T_4 = -30\,°C$), the graphical rate equations for different ["excess"] values were obtained and treated accordingly.[32] Then, the second-order rate constants $k_{obs}(T)$ at these temperatures were extracted from slopes of the corresponding "rate/[2] versus [1]" plots (Table 4 and Figure 13).

Table 4. Rate constants at various temperatures.

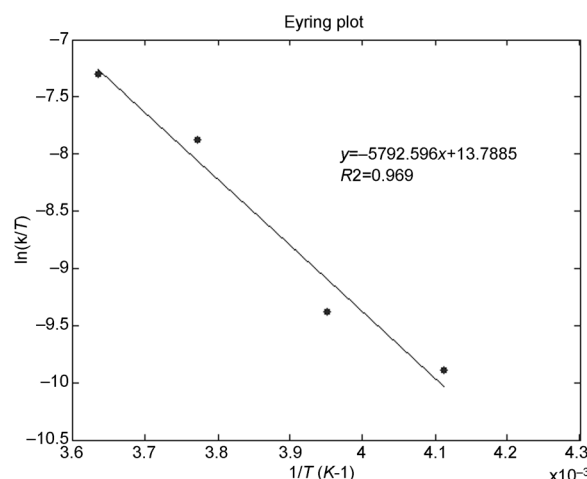| T [K]	243.15	253.15	265.15	275.15
k_{obs} [$M^{-1}s^{-1}$]	0.0125	0.0185	0.101	0.185

Figure 13. Construction of the Eyring plot and estimation of activation parameters of the fluorination/semi-pinacol reaction.

In the plot: $y = -5792.596x + 13.7885$, $R2 = 0.969$

With four values of the rate constant at four different temperatures now available, the activation parameters for the rate-determining step of the fluorination/semi-pinacol reaction were estimated by applying the Eyring equation [Eq. (3)], in which $k_B = 1.3806 \times 10^{-23}\ JK^{-1}$, $h = 6.626 \times 10^{-34}\ Js$ and $R = 8.31451\ JK^{-1}mol^{-1}$ are the Boltzmann, the Planck and the universal gas constants, respectively. These values are summarized below (assuming the transmission coefficient κ close to unity).

$$k_{obs} = \kappa\left(\frac{k_B T}{h}\right)e^{\left(\frac{-\Delta G^{\#}}{RT}\right)} \tag{3}$$

$\Delta H^{\#} = +11.5\ kcal\,mol-1$, $\Delta S^{\#} = -19.8\ eu$

Because $\Delta H^{\#} > T\Delta S^{\#}$, we can conclude that the fluorination/semi-pinacol reaction is under enthalpy control. Nevertheless, a large and negative entropy of activation provides a hint that the rate-determining step might be bimolecular. Considerable loss of translational and rotational degrees of freedom prior to collision might explain the entropy loss.
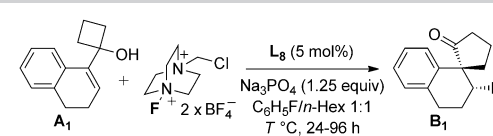
An alternative way of determining relative (as opposed to the absolute values obtained above) activation parameters involved measuring the enantiomeric excess of the fluorination/semi-pinacol reaction at different temperatures. For this study, the reactions were carried out under catalytic phase-transfer conditions (Table 5).[32]

By applying the Eyring equation [Eq. (3)] to the logarithm of the ratio of rate constants k_R and k_S, which correspond to the rates of formation of R and S enantiomers of product B_1, respectively, one obtains Equation (4). The various activation parameters of this equation are defined in Scheme 21.

$$\ln\left(\frac{k_R}{k_S}\right) = \frac{-\Delta\Delta G^{\#}}{RT} = \frac{-\Delta\Delta H^{\#}}{RT} + \frac{\Delta\Delta S^{\#}}{R} \tag{4}$$

$$\Delta\Delta G^{\#} = \Delta G_R^{\#} - \Delta G_S^{\#}$$

↖↖ These are not the final page numbers!

Table 5. Eyring analysis of enantioselectivity.
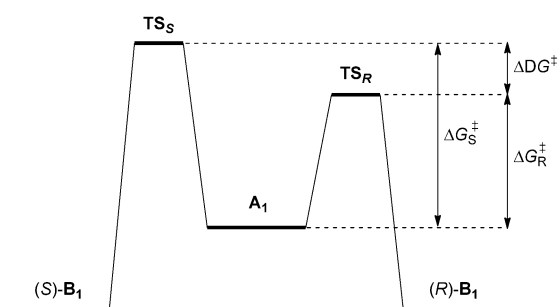

Entry[a]	T [°C]	e.r.[b]
1	−30	95.0:5.0
2	−20	94.8:5.2
3	−10	94.5:5.5
4	0	93.6:6.4
5	10	92.8:7.2
6	26	92.5:7.5
7	35	90.4:9.6
8	40	89.8:10.2

[a] Reaction conditions: a solution of allylic alcohol A_1 (0.20 mmol, 1.0 equiv), chiral phosphoric acid L_8 (0.02 mmol, 10 mol%), powdered Selectfluor (0.30 mmol, 1.5 equiv), and powdered Na_3PO_4 (0.25 mmol, 1.25 equiv) in anhydrous C_6H_5F/nHex 1:1 (total volume: 3.0 mL, 0.07 M) was stirred vigorously at the temperature stated for 24–96 h. [b] Determined by chiral HPLC analysis of purified compounds.

Figure 14. Eyring plot for the fluorination/semi-pinacol reaction.

Scheme 21. Gibbs free energies of activation for the Eyring analysis of enantioselectivity.

Furthermore, for the free-energy situation described in Scheme 21, and if first-order kinetics are assumed, the following relation holds [Eq. (5)].

$$\ln\left(\frac{k_R}{k_S}\right) = \ln\left(\frac{[\mathbf{B}_1^R]}{[\mathbf{B}_1^S]}\right) \tag{5}$$

Finally, by combining Equations (4) and (5), one gets a relation that links the enantiomer ratio of product $\mathbf{B}_1$ to the temperature [Eq. (6)].

$$\ln\left(\frac{[\mathbf{B}_1^R]}{[\mathbf{B}_1^S]}\right) = \ln(\text{e.r.}) = \frac{-\Delta\Delta G^{\#}}{RT} = \frac{-\Delta\Delta H^{\#}}{RT} + \frac{\Delta\Delta S^{\#}}{R} \tag{6}$$

Using Equation (6) and plotting ln(e.r.) versus $1/T$ gives a straight line the slope of which is $-\Delta\Delta H^{\#}/R$ and the intercept is $+\Delta\Delta S^{\#}/R$ (Figure 14).
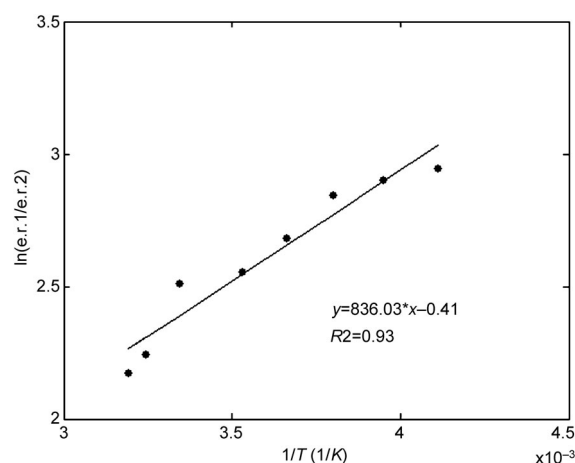
The following values for the differential enthalpy and entropy of activation were extracted from the slope and intercept, respectively: $\Delta\Delta H^{\#} = -1.66$ kcal mol^{-1} and $\Delta\Delta S^{\#} = -0.815$ eu. At $T_1 = -8$ °C (265 K, the "standard" temperature for the fluorination/semi-pinacol reaction), the entropy contribution to free energy of activation weights: $T\Delta\Delta S^{\#} = -0.216$ kcal mol$^{-1} < \Delta\Delta H^{\#}$. We can note an enthalpy control of enantioselectivity of the fluorination/semi-pinacol reaction. It is important to understand that this result concerns exclusively the enantioselectivity-determining step of the reaction. Furthermore, the obtained enthalpy and entropy values are not conclusive in an absolute sense, but solely represent the relative enthalpies/entropies of the transition structures leading to the R and S enantiomers of $\mathbf{B}_1$ ($\mathbf{TS}_R$ and $\mathbf{TS}_S$ in the nomenclature of Scheme 21). Nevertheless, this result is useful in concluding that the enthalpy term dominates the free-energy difference between the enantiomorphic transition structures. It is essentially this term that determined the sense of absolute induction of the whole process. Although small, the entropic contribution displays preference for the minor (S)-$\mathbf{B}_1$ enantiomer of the product.

Importantly, the above-described Eyring analysis of enantioselectivity deals exclusively with the enantioselectivity-determining step of the reaction. Additionally, because of the irreversibility of the C−F bond formation, the starting bimolecular collision event constitutes both the enantioselectivity as well as the rate-determining step of the fluorination/semi-pinacol reaction. Consequently, interfacial processes that occur prior to the actual chemical reaction are ignored.

Based on the obtained kinetic results alone, two plausible mechanistic scenarios capable of accounting for the experimentally observed rate law emerge: 1) the reaction is a fully concerted (but asynchronous) bimolecular process, and 2) the reaction is a two-step sequence involving an intermediate, in which the first step is rate-determining and bimolecular (Scheme 22). A fully concerted reaction would mean that the fluorination and the C−C bond migration both occur in a single step.
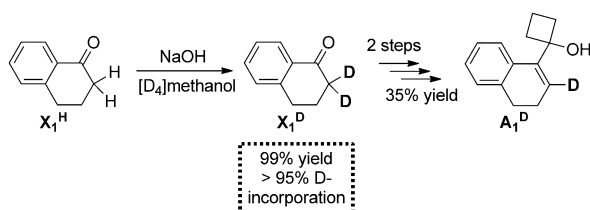
These two mechanistic proposals are kinetically indistinguishable and additional experiments were required to favour

These are not the final page numbers! ↗↗
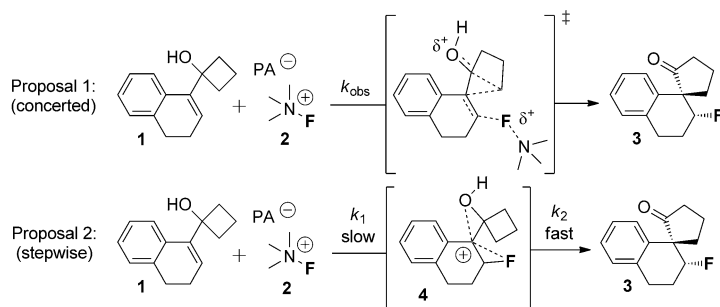
Scheme 22. Two kinetically indistinguishable mechanistic scenarios for the fluorination/semi-pinacol reaction.

one proposal over the other (vide infra). In this regard, one piece of information that could be helpful is what bonds have been broken, formed, or rehybridized during the rate-determining step.

Before tackling the investigation of kinetic isotopic effects in our fluorination/semi-pinacol reaction, an isotopically enriched deuterated version of the substrate allylic alcohol (A_1^D) had to be synthesized. Deuteration ($>95\%$ D-incorporation) was achieved by treating α-tetralone X_1^H with anhydrous NaOH in [D_4]MeOH as solvent (Scheme 23). The rest of the synthesis was processed in a manner identical to the non-deuterated substrate (A_1^H).

Scheme 23. Synthesis of the deuterated starting material A_1^D.

copy. All peaks were then integrated with normalization to the two reference peaks of 1,3,5-trimethoxybenzene ($\delta = 6.25$ and 3.32 ppm).[32]

Because the C–H/C–D bond in allylic alcohols A_1^H/A_1^D stays intact in the course of the fluorination/semi-pinacol reaction, a secondary KIE was expected. Furthermore, because secondary kinetic isotopic effects tend to be rather small, an appropriate method for measuring the KIE in our reaction was devised. It is important to note that as the reaction occurs, the reactants are incrementally enriched in the slower reacting component. Thus, for an isotopically enriched deuterated reactant, near the end of the reaction the proportion of the heavy isotope in the reactant will change relative to the proportion present at the beginning of the reaction. The isotopic content of the recovered starting material relative to the original starting material (R/R_0) is related to the extent of reaction (F) and the kinetic isotopic effect (KIE) through Equation (7).[35]

$$\frac{R}{R_0}(1-F)^{KIE-1} \tag{7}$$

When applying Equation (7) to three independent trials for measuring the KIE, the results summarized in Table 6 above were obtained. The mean value for the secondary kinetic isotopic effect being: $k_H/k_D = 0.77$.

The in-plane bending vibration (ca. 1350 cm^{-1}) is a much stiffer motion for the sp^2-hybridized carbon than is the out-of-plane bending mode (ca. 800 cm^{-1}). On the other hand, due to symmetry, the in-plane and out-of-plane bending modes for an sp^3-hybridized carbon atom are degenerate (both ca. 1350 cm^{-1}). Thus, since the in-plane bending vibrations are of almost the same energy for the two carbon hybrids, the major contribution to KIE is due to the difference in the out-of-plane mode frequency. The large difference in force constants for the out-of-plane bending mode of an sp^3-hybrid versus an sp^2-

With appropriate amounts of the deuterated substrate A_1^D in hand, the deuterium kinetic isotopic effect (KIE) was studied next. In the context of our fluorination/semi-pinacol reaction, the KIE was studied on the basis of a competition experiment between the protonated allylic alcohol A_1^H and its deuterated counterpart A_1^D. The isotopic content of the recovered starting material R at ca. 50% substrate conversion (F) was compared to the isotopic content of the original starting material R_0 (Table 6).

The isotopic content of the crude reaction mixtures was measured by ^{1}H NMR spectros-

Table 6. Determination of the secondary kinetic isotopic effect of the fluorination/semi-pinacol reaction.

Trial[a]	F[b]	R[b]	R_0[b]	R/R_0	KIE
1	0.44	0.57	0.50	1.14	0.77
2	0.46	0.57	0.50	1.14	0.79
3	0.47	0.59	0.50	1.18	0.74

[a] Reaction conditions: a solution of deuterated allylic alcohol A_1^D (0.10 mmol, 0.5 equiv) together with protonated allylic alcohol A_1^H (0.10 mmol, 0.5 equiv), chiral phosphoric acid L_8 (0.02 mmol, 10 mol%), powdered Selectfluor (0.30 mmol, 1.5 equiv), and powdered Na$_3$PO$_4$ (0.25 mmol, 1.25 equiv) in anhydrous C$_6$H$_5$F/nHex 1:1 (total volume: 3.0 mL, 0.07 M) was stirred vigorously at -20°C for 24 h. [b] Determined by ^{1}H NMR spectroscopic analysis of the crude reaction mixtures.

↖↖ **These are not the final page numbers!**

hybrid leads to a significant difference in the zero-point vibrational energy (*ZPE*) between C–H and C–D bonds in reactions that involve rehybridization between sp^3 and sp^2 carbon atoms. Furthermore, because an inverse ($k_H/k_D < 1$) secondary kinetic isotopic effect was found for our fluorination/semi-pinacol reaction, a rehybridization from sp^2 to sp^3 takes place in the transition structure of the rate-determining step (Scheme 24).
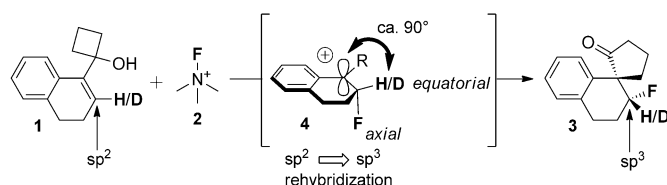
Scheme 24. Geometrical refinements of the transition structure using structural information provided by the KIE.

It is important to note that, since the observed secondary KIE effect is not attenuated by hyperconjugation in the intermediate carbocation **4**, we can conclude that the electrophilic fluorine atom approaches the allylic alcohol **1** by a pseudo-axial attack trajectory. Such a trajectory places the isotopically substituted C–H/C–D bond in a pseudo-equatorial position, which in turn makes it immune towards weakening by hyperconjugation with the vacant carbocationic *p*-orbital (dihedral angle of ca. 90°). In conclusion, we can state that the observation of a strong deuterium secondary kinetic isotopic effect not only reinforces the "intermediacy" of a carbocationic intermediate in the fluorination/semi-pinacol reaction, but also provides supplementary information regarding the geometry of the transition structure of the rate-determining step.

Up to this point of the manuscript, two types of experiments for studying the mechanism of our fluorination/semi-pinacol reaction were considered. First, the kinetics of the reaction were analyzed, which gave us useful information regarding the order of reactants involved in the mechanism prior to or during the rate-determining step. Second, the study of deuterium kinetic isotopic effects served to determine whether the bond to hydrogen has been rehybridized in the course of the reaction. Although very useful for global understanding of the mechanism, these experiments provided us with only limited structural information regarding the activated complex involved in the rate-de-

terming step. The study of substituent effects furnished this missing information.

Linear free-energy relationships (LFERs) were established on the basis of competition experiments between the unsubstituted allylic alcohol **A$_H$** and its *meta*- or *para*-substituted counterpart **A$_X$**. The ratio of rate constants k_X/k_H was approximated by the β-fluoro spiroketone product ratio [**B$_X$**]/[**B$_H$**] at approximately 50% conversion, which was in turn determined by ^{1}H and ^{19}F NMR spectroscopy (Table 7).[32] The experimentally-determined values for the substituent constants σ_m, σ_p and σ_p^+ were taken from Taft et al.[36]

LFER plots were then constructed using the simple Hammett relationship for rate constants [Eq. (8)][37] and three sets of Hammett substituent constants (σ_m, σ_p and σ_p^+).

$$\log\left(\frac{k_X}{k_H}\right) = \rho\sigma_X \tag{8}$$

A plot of the logarithm of the ratio of rate constants k_X/k_H versus total σ values (σ_m and σ_p) displayed considerable scatter, meaning that the *para*- and *meta*-substituents did not contribute in equal amounts to modulation of the electron density at the reaction site (upper left in Figure 15).

Important scatter was equally observed when plotting $\log(k_X/k_H)$ versus σ_m values (upper right plot in Figure 15). This experimental result suggests that the *meta*-substituents (X^m) do not influence the rate of the fluorination/semi-pinacol reaction as coherently as they do to the ionization of benzoic acid, presumably because direct resonance with the reaction site is not available from a *meta*-position. Nevertheless, a clear trend is seen, in which inductively electron-withdrawing substituents ($\sigma_m > 0$) such as F, Cl and OMe markedly retard the reaction when compared to the unsubstituted substrate (**A$_H$**). On the

Table 7. Hammett analysis of substituent effects of the fluorination/semi-pinacol reaction.

Entry[a]	Substituent (X)	σ_m	σ_p	σ_p^+	k_X/k_H[b]
1	*m*-Me	−0.07			1.18
2	*m*-OMe	+0.12			0.82
3	*m*-Cl	+0.37			0.40
4	*m*-F	+0.34			0.49
5	*p*-Me		−0.17	−0.31	3.57
6	*p*-OMe		−0.27	−0.78	8.75
7	*p*-Cl		+0.23	−0.11	0.61
8	*p*-F		+0.06	−0.07	1.26

[a] Reaction conditions: a solution of *meta*- or *para*-substituted allylic alcohol **A$_X$** (0.10 mmol, 0.5 equiv), together with **A$_H$** (0.10 mmol, 0.5 equiv), chiral phosphoric acid **L$_8$** (0.02 mmol, 10 mol%), powdered Selectfluor (0.30 mmol, 1.5 equiv), and powdered Na$_3$PO$_4$ (0.25 mmol, 1.25 equiv) in anhydrous C$_6$H$_5$F/nHex 1:1 (total volume: 3.0 mL, 0.07 M) was stirred vigorously at −20 °C for 24 h. [b] Determined by ^{1}H NMR spectroscopic analysis of the crude reaction mixtures.
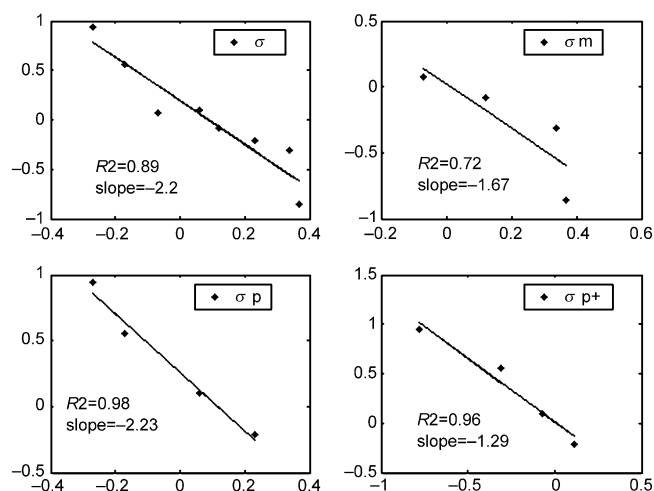
These are not the final page numbers! ↗↗

Figure 15. Hammett plots "log(k_X/k_H) versus σ" for three different sets of substituent constants (σ_m, σ_p and σ_p^+).

other hand, inductively electron-releasing substituents ($\sigma_m < 0$) such as the Me-group increase the rate of the reaction.

In sharp contrast to the situation observed for the log(k_X/k_H) versus σ_m plot, data scattering is considerably reduced when plotting the σ_p and σ_p^+ values as the x-axis (two bottom plots in Figure 15). This important observation constitutes a clear declaration on the importance of resonance effects in our fluorination/semi-pinacol reaction. This time, substituents capable of direct resonance with the reaction site, such as OMe and even F, accelerate the reaction markedly. The sensitivity constant extracted from the slope stands at: $\rho = -2.23$ for σ_p values, and $\rho^+ = -1.29$ for σ_p^+ values. These relatively large and negative sensitivity constants ρ and ρ^+ clearly indicate that positive charge is created at the reaction site in the transition structure of the rate-determining step.

Importantly, this experimental observation is most coherent with a stepwise mechanism for our fluorination/semi-pinacol reaction (Scheme 22). The intermediate carbocation invoked by the stepwise mechanism would then participate in direct resonance with the *para*-substituent, leading to rate enhancements for electron-releasing groups through stabilization of the transition state. Nevertheless, because the obtained sensitivity constants ρ and ρ^+ are not extremely large, a concerted but highly asynchronous mechanism cannot be fully ruled out.

Lastly, the absence of kinks or breaks in these Hammett plots suggests that a single reaction mechanism is operating across the entire set of substituents tested, and no change in the rate-determining step takes place.

Up to this point, the fluorination/semi-pinacol reaction was proposed to proceed through a rate-determining collision between the substrate allylic alcohol **1** and the lipophilic ion pair **2**. However, the exact structure of this "lipophilic ion pair" remained underexplored. The aim of the nonlinear effects study was to gain insight into the stoichiometry of this ionic fluorinating reagent.

It was already noted in the course of the kinetic study that successful preparation of the stoichiometric fluorinating re-

agent **2** required two equivalents of the lipophilic phosphate counterion **L₄** to be used.[32] Furthermore, the dicationic nature of the Selectfluor molecule imposes the association of two negatively charged species with it, as to compensate for the excessive electrostatic charge. Approaching this subject from a different angle, because the phosphate counterions **L₄** are chiral, an unequivocal proof that two such molecules associate with Selectfluor in the active fluorinating reagent could come from nonlinear behaviour of the fluorination/semi-pinacol reaction.

The study of nonlinear behaviour of the fluorination/semi-pinacol reaction commenced with preparation of a set of scalemic catalyst mixtures (R_a)-**L₄**/(S_a)-**L₄** with varying degrees of enantiomeric purity. To this end, enantiomerically pure phosphoric acids (R_a)-**L₄** and (S_a)-**L₄** were mixed in nine different proportions and the enantiomeric excesses of the resultant mixtures being confirmed by chiral HPLC after conversion to the corresponding methyl phosphates.[32] The obtained scalemic phosphate mixtures were subsequently employed as catalysts to promote the canonical fluorination/semi-pinacol reaction (Table 8).

A plot of ee_{prod} versus ee_{cat} revealed that a large and positive nonlinear effect operates in the fluorination/semi-pinacol reaction (Figure 16).

Fitting the experimental data to Kagan's ML₂ model [Eq. (9) and (10)][38] furnished the following values for the equilibrium constant (K) and the ratio of rates (g) parameters: $K = 99$, $g = 0.18$.

$$\beta = \frac{z}{x+y} = \frac{-Kee_{cat.}^2 + \sqrt{-4Kee_{cat.}^2 + K(4 + Kee_{cat.}^2)}}{4 + Kee_{cat.}^2} \quad (9)$$

$$ee_{prod} = ee_0 ee_{cat.} \frac{1+\beta}{1+g\beta} \quad (10)$$

By analogy, we have extended Kagan's model that deals with the interaction of a metal M with two chiral ligands L to our reaction, which involves one dicationic Selectfluor molecule (M) ion-paired with two chiral phosphate anions (L). Three different catalyst species, two homodimeric ion pairs (ML$_R$L$_R$ and ML$_S$L$_S$) and an heterodimeric *meso* ion pair (ML$_R$L$_S$), may be formed with relative concentrations x, y and z, respectively, which are interrelated by an equilibrium constant K (Scheme 25).

The parameters K and g provide hints about the nature of the active catalyst mixture. A value of $K = 99$ indicates that the heterodimeric *meso* ion pair ML$_R$L$_S$ is thermodynamically more stable than the two homodimeric ion pairs ML$_R$L$_R$ and ML$_S$L$_S$. Furthermore, a value of g less than 1 indicates that the *meso* species (which leads to racemic product) is a less active catalyst than are the enantiopure species for the fluorination/semi-pinacol reaction. Consequently, the *meso* ion pair ML$_R$L$_S$ acts as a thermodynamic "reservoir" that sequesters the (minor) homodimeric catalyst ML$_S$L$_S$, leaving only the (major) ML$_R$L$_R$ to react.

Taken together, these results suggest that two molecules of the chiral phosphate anion **L₄** are involved in the rate-deter-

↖↖ **These are not the final page numbers!**

Table 8. Nonlinear behaviour analysis of the fluorination/semi-pinacol reaction.

Entry[a]	ee_{cat} [%][b]	ee_{prod} [%][b]
1	0	0
2	23.0	51.6
3	43.6	70.4
4	46.6	78.4
5	58.8	80.4
6	72.8	87.4
7	82.2	87
8	100	90

[a] Reaction conditions: a solution of allylic alcohol A_1 (0.20 mmol, 1.0 equiv), scalemic phosphate mixture (R_a)-L_4/(S_a)-L_4 of optical purity ee_{cat} (0.02 mmol, 10 mol%), powdered Selectfluor (0.30 mmol, 1.5 equiv), and powdered Na_3PO_4 (0.25 mmol, 1.25 equiv) in anhydrous C_6H_5F/nHex 1:1 (total volume: 3.0 mL, 0.07 M) was stirred vigorously at $-20\,^\circ$C for 96 h. [b] Determined by chiral HPLC analysis of purified compounds.
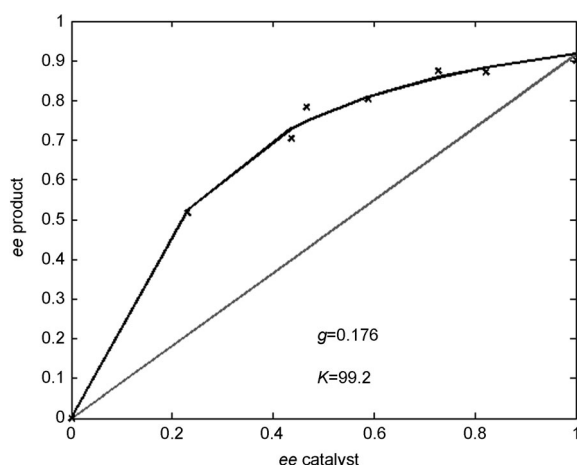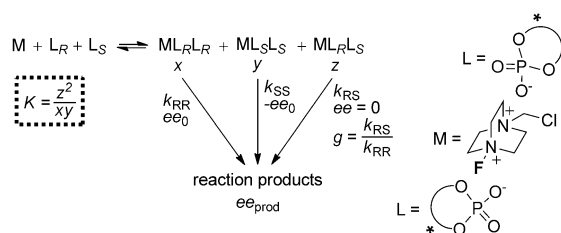

Figure 16. The relationship between the enantioselectivity of the fluorination/semi-pinacol reaction (ee_{prod}) and the enantiomeric excess of the chiral catalyst (ee_{cat}). The parameters K and g were obtained by fitting the data to Kagan's ML_2 model.

Scheme 25. ML_2 model developed by Kagan and co-workers, adapted to the fluorination/semi-pinacol reaction.

mining step of the fluorination/semi-pinacol reaction. Additionally, significant levels of chiral amplification (positive NLE) are observed, a fact that can be explained by high thermodynamic and kinetic stabilities of the heterochiral ion pair ML_RL_S. Although the product enantioselectivity is relatively high compared to the enantiopurity of the chiral catalyst, this comes at a cost of the overall reaction rate (note that the reaction time has been extended to 96 h).

Conclusions

In conclusion, in this manuscript we have described a highly enantioselective organocatalytic Wagner–Meerwein rearrangement of strained allylic alcohols A_x, initiated by an electrophilic halogenation event. All reactions were catalyzed by an ensemble of related chiral phosphoric acids $L_{6,8,9}$ derived from (R_a)-BINOL. The substrate scope encompasses allylic cyclopropanols, cyclobutanols and cyclopentanols, based on the dihydronaphthalene, indene, as well as the chromene scaffolds, with electron-releasing, electron-neutral, and moderately electron-withdrawing substituents at C5- and C6-positions. We have shown that the title reaction could be successfully extended to heavier halogen atoms (Br and I), provided that an appropriate achiral-reagent/chiral-counterion catalytic system was employed. All stereochemical assignments of the products were generously supported by X-ray crystallography.

Furthermore, β-fluoro spiroketones B_{11-16} were amenable to derivatization through a stereospecific Baeyer–Villiger oxidation, whereas β-iodo spiroketones $D_{8,9}$ were prone to stereospecific azide substitution, nicely demonstrating the synthetic relevance of the products.

Kinetic studies established that the fluorination/semi-pinacol reaction involved a bimolecular collision event between substrate alcohol A_1 and the chiral lipophilic ion pair as the rate-determining step. Moreover, the following activation parameters were established through Eyring analysis of temperature dependence of the reaction rate: $\Delta H^{\#} = +11.5$ kcal mol^{-1} and $\Delta S^{\#} = -19.8$ eu. Importantly, these values were obtained with comfortable confidence intervals, allowing for (at least) semi-quantitative conclusions to be drawn. One such conclusion being that the fluorination/semi-pinacol reaction is entropy-controlled.

Additionally, the observation of a significant *inverse* secondary kinetic isotopic effect ($k_H/k_D = 0.77$), as well as a large and negative Hammett sensitivity constant ($\rho = -2.2$) both favour a stepwise process, passing through an intermediate carbocation with significant rehybridation of the β-carbon at the transi-

tion state. Nevertheless, a fully concerted but highly asynchronous reaction mechanism could not be ruled out completely. Finally, the stoichiometry of the ionic fluorinating reagent was shown to involve two molecules of the chiral phosphate anion, as evidenced by the observation of significant positive nonlinear behaviour (positive NLE).

Acknowledgements

[1] For three recent reviews on asymmetric couterion-directed catalysis, see: a) M. Mahlau, B. List, *Angew. Chem. Int. Ed.* **2013**, *52*, 518–533; *Angew. Chem.* **2013**, *125*, 540–556; b) K. Brak, E. N. Jacobsen, *Angew. Chem. Int. Ed.* **2013**, *52*, 534–561; *Angew. Chem.* **2013**, *125*, 558–588; c) R. J. Phipps, G. L. Hamilton, F. D. Toste, *Nat. Chem.* **2012**, *4*, 603–614.

[2] For excellent reviews on chiral phosphoric acids catalysis, see: a) T. Akiyama, J. Itoh, K. Yokota, K. Fuchibe, *Angew. Chem. Int. Ed.* **2004**, *43*, 1566; b) G. Adair, S. Mukherjee, B. List, *Aldrichimica Acta* **2008**, *41*, 31–39; c) D. Uraguchi, M. Terada, *J. Am. Chem. Soc.* **2004**, *126*, 5356; d) M. Terada, *Synthesis* **2010**, 1929–1982; e) T. Akiyama, *Chem. Rev.* **2007**, *107*, 5744–5758.

[3] E. V. Anslyn, D. A. Dougherty in *Modern Physical Organic Chemistry*, University Science Books, Sausalitos, **2005**, pp. 164–180.

[4] a) A. Loupy, B. Tchoubar in *Salt Effects in Organic and Organometallic Chemistry*, 1st ed., VCH, Weinheim, Germany, **1992**; b) C. Reichardt in *Solvents and Solvent Effects in Organic Chemistry*, 3rd ed., VCH, Weinheim, Germany, **2002**.

[5] For excellent reviews on chiral quaternary ammonium salts catalysis, see: a) K. Maruoka in *Asymmetric Phase Transfer Catalysis*, Wiley-VCH, Weinheim, **2008**; b) I. Ojima in *Catalytic Asymmetric Synthesis*, Wiley-VCH, Weinheim, **2000**; c) K. Maruoka, T. Ooi, *Chem. Rev.* **2003**, *103*, 3013–3028; d) B. Lygo, B. I. Andrews, *Acc. Chem. Res.* **2004**, *37*, 518–525; e) T. Ooi, K. Maruoka, *Angew. Chem. Int. Ed.* **2007**, *46*, 4222–4266; *Angew. Chem.* **2007**, *119*, 4300–4345.

[6] U.-H. Dolling, P. Davis, E. J. J. Grabowski, *J. Am. Chem. Soc.* **1984**, *106*, 446–447.

[7] G. L. Hamilton, T. Kanai, F. D. Toste, *J. Am. Chem. Soc.* **2008**, *130*, 14984–14986.

[8] V. Rauniyar, A. D. Lackner, G. L. Hamilton, F. D. Toste, *Science* **2011**, *334*, 1681–1684.

[9] R. J. Phipps, K. Hiramatsu, F. D. Toste, *J. Am. Chem. Soc.* **2012**, *134*, 8376–8379.

[10] a) D. Lenoir, C. Chiappe, *Chem. Eur. J.* **2003**, *9*, 1036–1044; b) G. Bellucci, C. Chiappe, R. Bianchini, D. Lenoir, R. Herges, *J. Am. Chem. Soc.* **1995**, *117*, 12001–12002; c) S. E. Denmark, W. E. Kuester, M. T. Burk, *Angew. Chem. Int. Ed.* **2012**, *51*, 10938–10953; *Angew. Chem.* **2012**, *124*, 11098–11113.

[11] a) I. Roberts, G. E. Kimball, *J. Am. Chem. Soc.* **1937**, *59*, 947–948; b) G. A. Olah, J. M. Bollinger, *J. Am. Chem. Soc.* **1967**, *89*, 4744–4752; c) G. A. Olah, J. M. Bollinger, *J. Am. Chem. Soc.* **1968**, *90*, 947–953; d) G. A. Olah, J. M. Bollinger, J. Brinich, *J. Am. Chem. Soc.* **1968**, *90*, 2587–2594.

[12] a) G. Chen, S. Ma, *Angew. Chem. Int. Ed.* **2010**, *49*, 8306–8308; *Angew. Chem.* **2010**, *122*, 8484–8486; b) C. K. Tan, L. Zhou, Y. Yeung, *Synlett* **2011**, 1335–1339; c) S. A. Snyder, D. S. Treitler, A. P. Brucks, *Aldrichimica Acta* **2011**, *44*, 27–40.

[13] a) S. E. Denmark, M. T. Burk, *Org. Lett.* **2012**, *14*, 256–259; b) D. Huang, H. Wang, F. Xue, H. Guan, L. Li, X. Peng, Y. Shi, *Org. Lett.* **2011**, *13*, 6350–6353; c) G.-X. Li, Q.-Q. Fu, X.-M. Zhang, J. Jiang, Z. Tang, *Tetrahedron: Asymmetry* **2012**, *23*, 245–251; d) K. Murai, T. Matsushita, A. Nakamura, S. Fukushima, M. Shimura, H. Fujioka, *Angew. Chem. Int. Ed.* **2010**, *49*, 9174–9177; *Angew. Chem.* **2010**, *122*, 9360–9363; e) K. Murai, A. Nakamura, T. Matsushita, M. Shimura, H. Fujioka, *Chem. Eur. J.* **2012**, *18*, 8448–8453; f) S. E. Denmark, M. T. Burk, *Proc. Natl. Acad. Sci. USA* **2010**, *107*, 20655–20660; g) L. Zhou, C. K. Tan, X. Jiang, F. Chen, Y.-Y. Yeung, *J. Am. Chem. Soc.* **2010**, *132*, 15474–15476; h) C. K. Tan, L. Zhou, Y.-Y. Yeung, *Org. Lett.* **2011**, *13*, 2738–2741; i) C. K. Tan, C. Le, Y.-Y. Yeung, *Chem. Commun.* **2012**, *48*, 5793–5795; j) J. Chen, L. Zhou, Y.-Y. Yeung, *Org. Biomol. Chem.* **2012**, *10*, 3808–3811; k) J. Chen, L. Zhou, C. K. Tan, Y.-Y. Yeung, *J. Org. Chem.* **2012**, *77*, 999–1009; l) W. Zhang, S. Zheng, N. Liu, J. B. Werness, I. A. Guzei, W. Tang, *J. Am. Chem. Soc.* **2010**, *132*, 3664–3665; m) W. Zhang, N. Liu, C. M. Schienebeck, K. Decloux, S. Zheng, J. B. Werness, W. Tang, *Chem. Eur. J.* **2012**, *18*, 7296–7305.

[14] a) U. Hennecke, C. H. Müller, R. Fröhlich, *Org. Lett.* **2011**, *13*, 860–863; b) Y.-M. Wang, J. Wu, C. Hoong, V. Rauniyar, F. D. Toste, *J. Am. Chem. Soc.* **2012**, *134*, 12928–12931; c) G. E. Veitch, E. N. Jacobsen, *Angew. Chem. Int. Ed.* **2010**, *49*, 7332–7335; *Angew. Chem.* **2010**, *122*, 7490–7493; d) M. C. Dobish, J. N. Johnston, *J. Am. Chem. Soc.* **2012**, *134*, 6068–6071; e) A. Sakakura, A. Ukai, K. Ishihara, *Nature* **2007**, *445*, 900–903.

[15] O. Lozano, G. Blessley, T. Martinez del Campo, A. L. Thompson, G. T. Giuffredi, M. Bettati, M. Walker, R. Borman, V. Gouverneur, *Angew. Chem. Int. Ed.* **2011**, *50*, 8105–8109; *Angew. Chem.* **2011**, *123*, 8255–8259.

[16] a) D. C. Whitehead, R. Yousefi, A. Jaganathan, B. Borhan, *J. Am. Chem. Soc.* **2010**, *132*, 3298–3300; b) A. Jaganathan, A. Garzan, D. C. Whitehead, R. J. Staples, B. Borhan, *Angew. Chem. Int. Ed.* **2011**, *50*, 2593–2596; *Angew. Chem.* **2011**, *123*, 2641–2644; c) K. C. Nicolaou, N. L. Simmons, Y. Ying, P. M. Heretsch, J. S. Chen, *J. Am. Chem. Soc.* **2011**, *133*, 8134–8137; d) R. Yousefi, D. C. Whitehead, J. M. Mueller, R. J. Staples, B. Borhan, *Org. Lett.* **2011**, *13*, 608–611.

[17] a) S. Purser, P. R. Moore, S. Swallow, V. Gouverneur, *Chem. Soc. Rev.* **2008**, *37*, 320–330; b) D. O'Hagan, H. S. Rzepa, *Chem. Commun.* **1997**, 645–652; c) T. Furuya, A. S. Kamlet, T. Ritter, *Nature* **2011**, *473*, 470–477.

[18] a) G. W. Gribble, *Prog. Chem. Org. Nat. Prod.* **1996**, *68*, 1–423; b) N. Bell, L. Hsu, D. J. Jacob, M. G. Schultz, D. R. Blake, J. H. Butler, D. B. King, J. M. Lobert, E. Maier-Reimer, *J. Geophys. Res.* **2002**, *107*, ACH 8-1–ACH 8-12; c) C. Campagnuolo, E. Fattorusso, O. Taglialatela-Scafati, *Eur. J. Org. Chem.* **2003**, 284–287; d) F. Borrelli, C. Campagnuolo, R. Capasso, E. Fattorusso, O. Taglialatela-Scafati, *Eur. J. Org. Chem.* **2004**, 3227–3232.

[19] A. N. French, S. Bissmire, T. Wirth, *Chem. Soc. Rev.* **2004**, *33*, 354–362.

[20] B. M. Wang, L. Song, C. A. Fan, Y. Q. Tu, W. M. Chen, *Synlett* **2003**, 1497–1499.

[21] a) Z.-M. Chen, Q.-W. Zhang, Z.-H. Chen, H. Li, Y.-Q. Tu, F.-M. Zhang, J.-M. Tian, *J. Am. Chem. Soc.* **2011**, *133*, 8818–8821; b) H. Li, F.-M. Zhang, Y.-Q. Tu, Q.-W. Zhang, Z.-M. Chen, Z.-H. Chen, J. Li, *Chem. Sci.* **2011**, *2*, 1839–1841.

[22] M. Wang, B. M. Wang, L. Shi, Y. Q. Tu, C.-A. Fan, S. H. Wang, X. D. Hu, S. Y. Zhang, *Chem. Commun.* **2005**, 5580–5582.

[23] F. Romanov-Michailidis, L. Guénée, A. Alexakis, *Angew. Chem. Int. Ed.* **2013**, *52*, 9266–9270; *Angew. Chem.* **2013**, *125*, 9436–9440.

[24] For the first report on the employment of the TRIP phosphoric acid, see: M. Klussmann, L. Ratjen, S. Hoffmann, V. Wakchaure, R. Goddard, B. List, *Synlett* **2010**, 2189–2192.

[25] L. Simón, J. M. Goodman, *J. Org. Chem.* **2011**, *76*, 1775–1788.

[26] I. Ćorić, S. Vellalath, B. List, *J. Am. Chem. Soc.* **2010**, *132*, 8536–8537.

[27] F. Romanov-Michailidis, M. Pupier, L. Guénée, A. Alexakis, *Chem. Commun.* **2014**, *50*, 13461–13464.

[28] A. A. Neverov, R. S. Brown, *J. Org. Chem.* **1998**, *63*, 5977–5982.

[29] a) R. S. Brown, R. W. Nagorski, A. J. Bennet, R. E. D. McClung, G. H. M. Aarts, M. Klobukowski, R. McDonald, B. D. Santarsiero, *J. Am. Chem. Soc.* **1994**, *116*, 2448–2456; b) A. A. Neverov, R. S. Brown, *J. Org. Chem.* **1996**, *61*, 962–968; c) R. S. Brown, *Acc. Chem. Res.* **1997**, *30*, 131–137.

[30] For a recent review on azide chemistry, see: S. Bräse, C. Gil, K. Knepper, V. Zimmermann, *Angew. Chem. Int. Ed.* **2005**, *44*, 5188–5240; *Angew. Chem.* **2005**, *117*, 5320–5374.

[31] a) P. L. Rinaldi, *J. Am. Chem. Soc.* **1983**, *105*, 5167–5168; b) C. Yu, G. C. Levy, *J. Am. Chem. Soc.* **1984**, *106*, 6533–6537.

[32] See the Supporting Information for details.

[33] F. Romanov-Michailidis, L. Guénée, A. Alexakis, *Org. Lett.* **2013**, *15*, 5890–5893.

[34] D. G. Blackmond, *Angew. Chem. Int. Ed.* **2005**, *44*, 4302–4320; *Angew. Chem.* **2005**, *117*, 4374–4393.

◤◤ These are not the final page numbers!

[35] D. A. Singleton, A. A. Thomas, *J. Am. Chem. Soc.* **1995**, *117*, 9357–9358.
[36] C. Hansch, A. Leo, R. W. Taft, *Chem. Rev.* **1991**, *91*, 165–195.
[37] A. Williams in *Free Energy Relationships in Organic and Bio-Organic Chemistry*, **2003**, Royal Society of Chemistry, Cambridge, England.
[38] a) C. Puchot, O. Samuel, E. Dunach, S. Zhao, C. Agami, H. B. Kagan, *J. Am. Chem. Soc.* **1986**, *108*, 2353–2357; b) D. Guillaneux, S. H. Zhao, O. Samuel, D. Rainford, H. B. Kagan, *J. Am. Chem. Soc.* **1994**, *116*, 9430–9439.
[39] F. Romanov-Michailidis, M. Pupier, C. Besnard, T. Bürgi, A. Alexakis, *Org. Lett.* **2014**, *16*, 4988–4991.
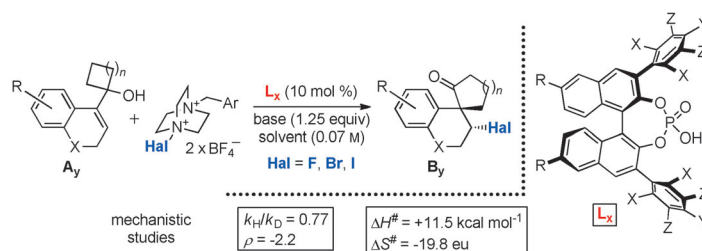
FULL PAPER

Reaction Mechanism

F. Romanov-Michailidis,
M. Romanova-Michaelides, M. Pupier,
A. Alexakis*

■■ – ■■

Enantioselective Halogenative Semi-Pinacol Rearrangement: Extension of Substrate Scope and Mechanistic Investigations

Scope and limitations of the fluorination-initiated semi-pinacol rearrangement of strained, prochiral allylic alcohols are described. This reaction is proposed to operate through anionic phase-transfer technology, and can be readily extended the heavier halogen (Br, I) congeners. In comparison with the fluorination reaction, an intriguing inversion of the sense of absolute induction for the heavier halogens is described (see scheme).